J. Fluid Mech. (2001), *vol.* 426, *pp.* 355–386. Printed in the United Kingdom

Steady-state flows in an enclosure ventilated by buoyancy forces assisted by wind

By G. R. HUNT† AND P. F. LINDEN‡

Department of Applied Mathematics and Theoretical Physics, University of Cambridge, Silver Street, Cambridge, CB3 9EW, UK

(Received 10 March 1998 and in revised form 7 July 2000)

We examine ventilation driven by a point source of buoyancy on the floor of an enclosure in the presence of wind. Ventilation openings connecting the internal and external environment are at high level on the leeward façade and at low level on the windward façade, so that the wind-driven flow in the enclosure is in the same sense as the buoyancy-driven flow. We describe laboratory experiments that determine the parameters controlling the ventilation under these conditions and compare the results with predictions of a theoretical model.

Previous work has shown that when ventilation is driven solely by a single localized source of buoyancy flux B, a stable, two-layer stratification and displacement flow forms. The steady height of the interface, between the buoyant upper layer and the lower layer at ambient density ρ, is independent of B and depends only on the 'effective' area A^* of the openings, the height H of the enclosure and entrainment into the plume.

For wind-assisted flows, the ventilation is increased owing to the wind pressure drop Δ between the windward and leeward openings. The two-layer stratification and displacement flow are maintained over a range of wind speeds, even when the wind-induced flow far exceeds the flow induced by the buoyancy force. The steady height of the interface depends upon the Froude number $Fr = (\Delta/\rho)^{1/2}(H/B)^{1/3}$ and the dimensionless area of the openings A^*/H^2. Increasing the wind speed raises the position of the interface and decreases the temperature of the upper layer (as does increasing A^*/H^2), while increasing B lowers the level of the interface and increases the temperature of the upper layer. For significantly larger Fr, the displacement flow breaks down and we investigate some aspects of this breakdown. The implications of these flows to passive cooling of a building by natural ventilation are discussed.

1. Introduction

A major part of energy expenditure in modern buildings is due to air conditioning and other mechanical means of ventilation. Operating correctly, naturally ventilated buildings typically consume less than a third of the energy of comparable air-conditioned buildings (Energy Consumption Guide 19, Best Practice Programme, Energy Efficiency in Offices, BRESCU, Energy Efficiency Office, October 1991). Natural ventilation is driven by wind, and buoyancy forces associated with density

† Present address: Department of Civil & Environmental Engineering, Imperial College of Science, Technology and Medicine, London SW7 2BU, UK.

‡ Present address: Department of Mechanical & Aerospace Engineering, University of California, San Diego, 9500 Gilman Drive, La Jolla, CA 92093-0411, USA.

differences between the internal and external environment. In buildings, the density contrast is usually generated by temperature differences but may also arise due to a difference in composition, e.g. in a building filled with smoke, or due to a release of a chemical substance, e.g. natural gas. Flows in buildings driven by density differences are commonly referred to as stack-driven flows, and they may be enhanced by increasing the density contrast between the internal and external environment, by increasing the height between the inlet and outlet openings (the stack), by increasing the area of the vents, or by suitably harnessing the force of the wind. The flow of wind around a building produces a dynamic (or wind) pressure distribution over its external surface with, in general, positive wind pressures on the windward façades and negative wind pressures in the lee and in regions of flow separation. By locating ventilation openings in regions of positive and negative pressures, the wind may be harnessed to drive a flow in the interior. The driving force produced by the wind is free and buoyancy-driven ventilation is typically produced by heat gains from solar radiation, occupants, machinery, electrical equipment, etc., or as a consequence of warming the air inside the space in order to provide comfort for the occupants. Natural ventilation has, therefore, the potential to provide an energy efficient means of ventilating a space.

To be effective, a natural ventilation system must meet specific requirements for the supply of fresh air throughout the year. These requirements are normally to provide fresh air for respiration and for the removal of carbon-dioxide, odours and excess heat. In winter these requirements can usually be met with relatively low ventilation flow rates, and in office spaces typically $8\,\mathrm{l\,s^{-1}}$ of air per person are recommended (Building Regulations: part F1 (Ventilation) HMSO, 1991). In summer the main requirement of a natural ventilation system is to remove excess heat in order to maintain internal air temperatures at comfortable levels. Non-domestic buildings typically experience the largest heat gains during the occupied daylight hours, when the need for ventilation is greatest, and minimal gains at night when the space is unoccupied. Different natural ventilation strategies may be adopted depending upon the seasonal or diurnal requirements. For example, if cool air is introduced at high level it will tend to mix with the air in the space. This *mixing ventilation* can be used to temper the ambient air and it provides fairly low ventilation rates. If cool air is introduced at low level, displacing warm air out through openings at high levels – *displacement ventilation* – larger ventilation rates are produced.

In this paper, we focus attention on displacement ventilation for which the ventilation rate is determined by the areas of the upper and lower openings and the vertical distance separating them, the temperature and depth of the warm upper zone, and the driving produced by the wind. A key consideration in the design of stack-driven naturally ventilated buildings is the depth and temperature of the warm upper zone; it must be maintained at a depth sufficient to drive the required flow through the building, while ensuring it is above the occupied levels. If the openings are too small or if their locations are not appropriately chosen, the warm layer may descend to the occupied regions. This can have a strong deleterious effect on indoor air quality as occupants are then exposed to the higher air temperatures and pollutant levels in the upper layer. The sizes and location of the ventilation openings must therefore be selected to ensure this balance is maintained.

Experiments, using small-scale laboratory models in water tanks, and theoretical modelling has been conducted over the past few years to address these and other fundamental problems associated with natural ventilation. A review of this research is given by Linden (1999). The aim is to gain an improved understanding of the physics

of air flows in buildings and to develop simple design guidelines for energy-efficient ventilation systems. The work presented in this paper contributes to this research and we place our study in context with a brief summary of the previous results.

Natural ventilation driven solely by buoyancy forces is discussed by Linden, Lan-Serff & Smeed (1990). They consider transient displacement and mixing flows in a ventilated space of height H that initially contains fluid of a different density than its surroundings. Steady-state flows driven by a continuous source of buoyancy are also considered. When openings of area a_t and a_b are made in the top and bottom faces, respectively, Linden *et al.* (1990) show these areas may be combined and expressed as an 'effective' opening area A^*, where

$$A^* = \frac{C_D a_t a_b}{(\frac{1}{2}((C_D^2/C_e)a_t^2 + a_b^2))^{1/2}} \tag{1}$$

(see also Cooper & Linden 1996). The quantities C_e and C_D are the coefficients of expansion and discharge, respectively, and represent the energy losses associated with fluid flowing through the inlet and outlet openings. Linden *et al.* (1990) show that displacement ventilation driven by a continuous point source of buoyancy on the floor of the space produces a steady stratification consisting of two homogeneous fluid layers separated by a horizontal interface at a height h above the floor. The steady level of the interface is given by the height at which the volume and buoyancy fluxes through the upper openings equal that supplied to the upper layer by the source. The lower layer is at ambient temperature and the upper layer has a temperature equal to the plume temperature at height h. Of the three independent quantities controlling the flow, namely, A^*, H and B, the buoyancy flux B is the only quantity containing the dimensions of time, and hence, the steady-state position of the interface is independent of B. This result is confirmed by experiment. In order to determine h, Linden *et al.* (1990) equate the volume flux, driven by a buoyant fluid layer of depth $H-h$, and reduced gravity g' with the volume flux and reduced gravity in the rising turbulent plume at the height h. A key result of this work is that the ambient layer depth h is determined by entrainment into the rising plume, and can be increased only by increasing the dimensionless area A^*/H^2 of the openings. The dimensionless interface height $\xi = h/H$ is given by

$$\frac{A^*}{H^2} = C^{3/2}\left(\frac{\xi^5}{1-\xi}\right)^{1/2}, \tag{2}$$

where $C = 6\alpha(9\alpha/10)^{1/3}\pi^{2/3}/5$ is a parameter dependent upon the 'top-hat' entrainment coefficient α for the plume. Increasing B increases the temperature step across the interface and, consequently, the volume flow rate through the space.

Cooper & Linden (1996) examine steady-state displacement ventilation produced by two non-interacting plumes of unequal strengths B_1 and B_2. In this case, a three-layer stratification is produced and the heights of the interfaces are determined solely by A^*/H^2 and the buoyancy flux ratio B_1/B_2. The depth of the stratified zone was again found to be independent of the total buoyancy flux supplied to the enclosure. Linden & Cooper (1996) confirm that the latter result holds for any number of non-interacting buoyant sources.

On most days natural ventilation is driven by the combined forces of wind and buoyancy, and even at moderate wind speeds a simple consideration of the respective pressure differences (Hunt & Linden 1999) suggests that the wind apparently provides the dominant driving force. Hunt & Linden (1996) show that transient displacement

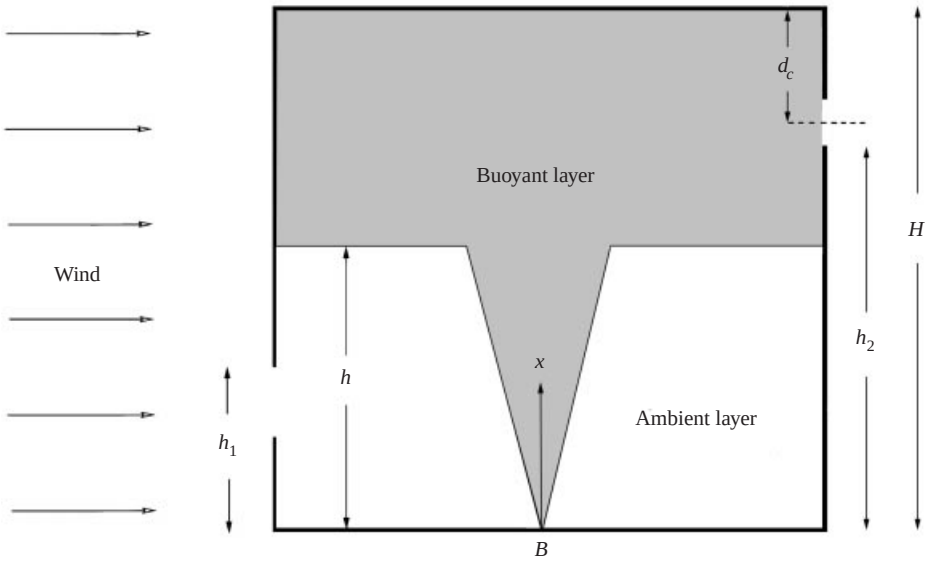

FIGURE 1. Displacement flow in an enclosure; the upper (leeward) and lower (windward) openings are located so that wind and buoyancy forces assist one another to ventilate the space.

flows as established by an initial density contrast between the interior and exterior environments (in the absence of a continuous buoyancy source) are significantly enhanced if the buoyancy-driven flow is assisted by wind. Even on a windy day, however, the buoyancy force may still have a significant effect on air movement and stratification by setting the flow patterns within the space (Hunt & Linden 1996, 1999).

In this paper we extend the work of Linden *et al.* (1990) by considering steady-state natural ventilation flows which are driven by buoyancy forces assisted by wind. Laboratory experiments and theoretical modelling have been used to determine the variation in temperature, stratification and flow rate as a function of the wind speed, strength of the buoyancy source, area of the openings and height of the space. The paper is set out as follows. A mathematical model is presented in § 2. Laboratory experiments designed to illustrate these flows and compare with the theory are described in § 3. The results of these experiments are presented in § 4 and comparisons made with the theoretical predictions of § 2. The implications of these flows for building design and ventilation strategies are discussed in § 5 and conclusions are drawn in § 6.

2. A mathematical model

Connections between the enclosure and the ambient are via openings at low level in regions of positive wind pressure (e.g. on the windward face) and at high level in regions of negative wind pressure (e.g. on the leeward face or on the roof of the enclosure). The areas of the windward and leeward openings are denoted by a_W and a_L, respectively. Figure 1 shows such an enclosure and the notation used. Internal heat gains, representative of a localized source of heat are modelled as a point source, of buoyancy flux B, on the floor. The vertical distance between the source and the ceiling is denoted by H and the cross-sectional area of the enclosure is assumed to be sufficiently large so that the rising plume does not extend to the sidewalls and is able to entrain freely.

In the absence of wind, buoyant fluid rises from the source as a turbulent plume,

entraining fluid from its surroundings and increasing in density. When the plume reaches the ceiling it spreads horizontally to the sides of the enclosure and creates a layer of buoyant fluid as depicted in figure 1. The difference in hydrostatic pressure between the upper and lower openings inside the space is then less than between the same heights in the external ambient fluid. Consequently, the buoyant layer drives a flow through the space. Buoyant fluid flows out through the upper openings and an equal volume of denser, ambient fluid enters through the lower openings; a displacement flow and a two-layer stratification is established (Linden *et al.* 1990). Before a steady flow is reached the volume flux through the enclosure increases as the depth and total buoyancy of the upper layer increase. The layer of buoyant fluid will continue to increase in depth and reduce in density (Hunt & Linden 1998) until the volume flux of fluid it drives through the enclosure is equal to the volume flux in the plume at the level of the interface. When a steady state is reached, there is no net buoyancy flux into the upper layer, which is then of uniform density equal to that in the plume at the level of the interface.

Wind subjects the fluid inside the enclosure to an additional driving force associated with the dynamic pressure drop Δ between the windward and leeward openings. In the case considered here, where the windward openings are at low level and the leeward openings are at high level, the wind assists the buoyancy-driven flow (Hunt & Linden 1996, 1999). For the purposes of this analysis it is assumed that the flow maintains the same basic two-layer structure – this is observed to be the case for a wide range of wind speeds and buoyancy fluxes (see § 4). The increased flow through the enclosure driven by the wind causes the interface to rise to a new level where the volume flux in the plume is equal to the volume flux produced by the buoyancy and wind. A steady-state displacement flow is then re-established. To determine the steady-state height h of the interface we extend the method adopted by Linden *et al.* (1990). We assume 'top-hat' profiles for the density and velocity across the plume and, at height h, equate the volume flux and reduced gravity in the rising turbulent plume with the volume flux driven through the space by a buoyant fluid layer of density difference $\rho - \Delta\rho$ subject to a wind pressure drop Δ. The density of the buoyant layer is determined by equating it with the density of the plume at the level of the interface.

We first determine the ventilation driven through an enclosure containing a given two-layer stratification and exposed to wind. At this stage a continuous buoyancy source is not present. A theoretical model for such a flow, i.e. the transient, wind-assisted displacement of buoyancy fluid from a ventilated space which is surrounded by denser fluid, is presented by Hunt & Linden (1999). The total volume flow rate Q through the space is given by summing the wind and buoyancy-driven flows in quadrature

$$Q = (Q_W^2 + Q_B^2)^{1/2}, \tag{3}$$

where the respective wind- and buoyancy-produced volume fluxes are

$$Q_W = A^* \left(\frac{\Delta}{\rho}\right)^{1/2} \quad \text{and} \quad Q_S = A^*(g'(H - h - d_c))^{1/2}. \tag{4a,b}$$

Here $(H - h - d_c)$ is the useful depth of the buoyant layer, d_c denotes the vertical distance between the midpoint of the upper opening and the top of the space (figure 1), and A^* is the 'effective' area of the openings of the same form as (1),

$$A^* = a_W a_L \left(\frac{2C_e C_D^2}{C_e a_W^2 + C_D^2 a_L^2}\right)^{1/2}. \tag{5}$$

A derivation of (3)–(5) is presented in Appendix A. The expansion and discharge

coefficients, C_e and C_D, respectively, can be determined by detailed examination of the flow through an opening. Batchelor (1967, p. 390) shows that except for some peculiar shaped openings C_e lies between 0.5 (for sharp-edged openings) and 1 (for smooth openings). Ward-Smith (1980, p. 395) suggests that for square-edged openings that occupy less than approximately 50% of the cross-sectional area of the approach duct $C_D \approx 0.6$; this value is confirmed by Flourentzou, Mass & Roulet (1996) who made measurements of the flow through typical building ventilation openings. In this paper we shall take $C_e = 0.5$ and $C_D = 0.6$.

The density difference $\Delta\rho$ between the fluid in the homogeneous buoyant upper layer and the surrounding fluid, of density ρ, is assumed to be small so that the Boussinesq approximation is valid and $g' = g\Delta\rho/\rho$ denotes the reduced gravity. Assuming top-hat profiles for the density and velocity across the plume, the buoyancy and volume fluxes, B and Q_P, respectively, and the reduced gravity G', for a turbulent buoyant plume issuing from a point source in a large body of stationary, unstratified fluid, are given by

$$B = Q_p G' = \text{constant}, \tag{6a}$$

$$Q_p(x, B) = C(Bx^5)^{1/3}, \tag{6b}$$

$$G'(x, B) = (B^2 x^{-5})^{1/3}/C \tag{6c}$$

(Morton, Taylor & Turner 1956), where x denotes the vertical distance from the source. A range of values for the entrainment coefficient are quoted in the literature. Morton *et al.* (1956) found that a value of $\alpha_G = 0.093$ agreed well with their experimental observations, while experiments by Baines (1983) yielded $\alpha_G = 0.074$ (the subscript is used here to refer to entrainment coefficients for Gaussian profiles). These two values of α_G lie towards the upper and lower limits of the reported range and there is uncertainty regarding the most appropriate value. Turner (1986) suggested that $\alpha_G = 0.083$ is a suitable empirical value and we shall adopt this value in the present model. For top-hat profiles we therefore have $\alpha = \sqrt{2}\alpha_G \approx 0.117$. The sensitivity of the predictions of interface height and reduced gravity in ventilated spaces to α_G are examined in § 4.

Equating the total volume flux (3) with the volume flux (6*b*) in the plume at the height of the interface (i.e. at $x = h$) gives

$$A^* \left(g'(H - h - d_c) + \frac{\Delta}{\rho} \right)^{1/2} = C B^{1/3} h^{5/3}. \tag{7}$$

Similarly, equating reduced gravities at the interface level gives the reduced gravity g' of the upper layer, namely

$$g' = G'(x = h, B) = \frac{(B^2 h^{-5})^{1/3}}{C}. \tag{8}$$

The change in density $\Delta\rho$ across the interface is therefore

$$\Delta\rho = \frac{\rho(B^2 h^{-5})^{1/3}}{gC}. \tag{9}$$

Substituting for g' from (8) into (7) and introducing the non-dimensional interface height $\xi = h/H$ yields

$$\frac{A^*}{H^2} = \frac{C^{3/2}\xi^{5/3}}{((1 - \xi - d_c/H)/\xi^{5/3} + CFr^2)^{1/2}}, \tag{10}$$

where the Froude number Fr, defined as

$$Fr = \sqrt{\frac{\Delta/\rho}{(B/H)^{2/3}}}, \tag{11}$$

is a measure of the relative magnitudes of the wind- and buoyancy-produced velocities. For $Fr \ll 1$ buoyancy forces are dominant while for $Fr \gg 1$ wind forces dominate. Equation (10) predicts that, for natural ventilation driven by buoyancy forces assisted by wind, the position of the interface is dependent upon entrainment into the plume, the strength B of the source, the wind pressure drop Δ and the dimensionless area of the openings A^*/H^2. This is in contrast to flows driven by buoyancy forces alone where the position of the interface is independent of B and depends only upon entrainment into the plume and A^*/H^2. For an enclosure of fixed height H, (11) shows that increasing the Froude number is equivalent to increasing the dynamic pressure drop between the openings, i.e. increasing the wind speed, or decreasing the strength of the source. Note that when ventilation openings are made in the bottom and top of the enclosure (i.e. $d_c/H = 0$) and in the absence of wind, (10) reduces to (2) derived by Linden *et al.* (1990) for flows driven by buoyancy forces alone. For n equal non-interacting plumes (10) becomes

$$\frac{A^*}{nH^2} = \frac{C^{3/2}\xi^{5/3}}{((1-\xi-d_c/H)/\xi^{5/3} + CFr^2)^{1/2}}. \tag{12}$$

In order to determine the volume flow rate Q through the space and the reduced gravity g' of the upper layer it is convenient, for a variable dynamic pressure drop, to introduce the scalings

$$\frac{Q}{B^{1/3}H^{5/3}} = C\xi^{5/3} \tag{13}$$

and

$$\frac{g'}{G'_H} = \xi^{-5/3}, \tag{14}$$

where $G'_H = G'(x = H, B)$ is the reduced gravity of the plume at the ceiling. For a variable source strength we introduce the scalings

$$\frac{Q}{H^2(\Delta/\rho)^{1/2}} = CFr^2\xi^{5/3} \tag{15}$$

and

$$\frac{g'}{(\Delta/\rho H)} = CFr^{-2}\xi^{-5/3}. \tag{16}$$

These scalings are used in the graphical presentation of the results that follow. However, the relative effects of buoyancy and wind on the other properties of the system are not uniquely related to h/H. For example, the dependence of Q on B, Δ, h and A^* may be obtained directly from (3) and (4) where on substituting $g' = B/Q$ we obtain

$$Q^3 - \left(A^{*2}\frac{\Delta}{\rho}\right)Q - BA^{*2}(H-h-d_c) = 0. \tag{17a}$$

It is convenient to express the flow rate Q as a dimensionless variable in terms of the wind-driven component Q_W, see (4*a*), as

$$\left(\frac{Q}{Q_W}\right)^3 - \frac{Q}{Q_W} = \frac{1}{Fr^3}\frac{H^2}{A^*}(1-\xi-d_c/H), \tag{17b}$$

and in terms of the buoyancy-driven component $Q_B = [A^{*2}B(H-h-d_c)]^{1/3}$ as

$$\left(\frac{Q}{Q_B}\right)^3 - \left(\frac{A^*}{H^2}\right)^{2/3} \frac{Fr^2}{(1-\xi-d_c/H)}\frac{Q}{Q_B} = 1. \tag{17c}$$

Equations (17*b*) and (17*c*) show that the flow Q through the space depends not only on the Froude number Fr but also on the wind driving Δ and the stack driving B separately. If Q_W is held fixed (by fixing Δ) then (17*b*) shows that Q decreases with increasing Fr. For fixed Δ, increases in Fr are produced by decreasing B. Conversely, (17*c*) shows that when Q_B is fixed, the flow rate Q increases with increasing Fr, which is achieved by increasing Δ. This behaviour is in accord with expectations. Increasing Fr, to say $Fr = Fr_1$, by increasing Δ for fixed B raises the interface and implies a greater wind-driven component and, hence, a larger Q. Obtaining the same Froude number, i.e. Fr_1, by holding Δ fixed and decreasing B, also raises the interface but reduces the buoyancy-driven component and, hence, decreases Q. This latter behaviour is still consistent with the flux across the interface being carried in the plume because, although the plume crosses the interface further from the source, the volume flux in the plume is still lower since B is less (see (6*b*)).

The theoretical model (10)–(16) is valid only while the interface lies between the upper and lower openings, i.e. for

$$\xi_{\min} = \frac{h_1}{H} < \xi < \frac{h_2}{H} = \xi_{\max}, \tag{18}$$

where h_1 is the distance between the floor and the top of the lower openings, and h_2 is the distance between the floor and the bottom of the upper openings (figure 1). This constraint determines the ranges of Fr and A^*/H^2 over which the model holds; for a fixed value of Fr, (18) is satisfied if

$$\frac{C^{3/2}\xi_{\min}^{5/3}}{(\gamma_{\min}+CFr^2)^{1/2}} < \frac{A^*}{H^2} < \frac{C^{3/2}\xi_{\max}^{5/3}}{(\gamma_{\max}+CFr^2)^{1/2}}, \tag{19a}$$

and for a fixed value of A^*/H^2, (18) is satisfied if

$$\sqrt{\frac{1}{C}\left(\frac{C^3\xi_{\min}^{10/3}}{(A^*/H^2)^2} - \gamma_{\min}\right)} < Fr < \sqrt{\frac{1}{C}\left(\frac{C^3\xi_{\max}^{10/3}}{(A^*/H^2)^2} - \gamma_{\max}\right)}, \tag{19b}$$

where

$$\gamma_{\min} = \frac{1-\xi_{\min}-d_c/H}{\xi_{\min}^{5/3}} \quad \text{and} \quad \gamma_{\max} = \frac{1-\xi_{\max}-d_c/H}{\xi_{\max}^{5/3}}. \tag{19c,d}$$

The consequences of these constraints are examined in § 4.

Predictions of the effect of the wind on the buoyancy-driven displacement flow are now examined. The dimensions of the experimental box described in § 4, in which these flows were reproduced at small scale in the laboratory, imply $d_c/H = 8.6\times10^{-2}$ and we use this value below. The effect of Fr on the steady-state flow inside the enclosure is shown in figure 2, which plots (*a*) h/H, (*b*) g'/G'_H and (*c*) $Q/(B^{1/3}H^{5/3})$ as functions of A^*/H^2 for $Fr = \{0, 1, 2, 4, 8, 16\}$. The plots show that, for a given A^*/H^2, the depth of the ambient layer increases as Fr is increased (figure 2*a*); the upper layer decreases in depth and increases in density (it cools) as it is fed by less buoyant fluid from the plume. The density contrast across the interface therefore decreases (figure 2*b*) and there is an increased flow rate through the space (figure 2*c*). A decrease in both the depth and density of the upper layer with increasing Fr results in a reduction

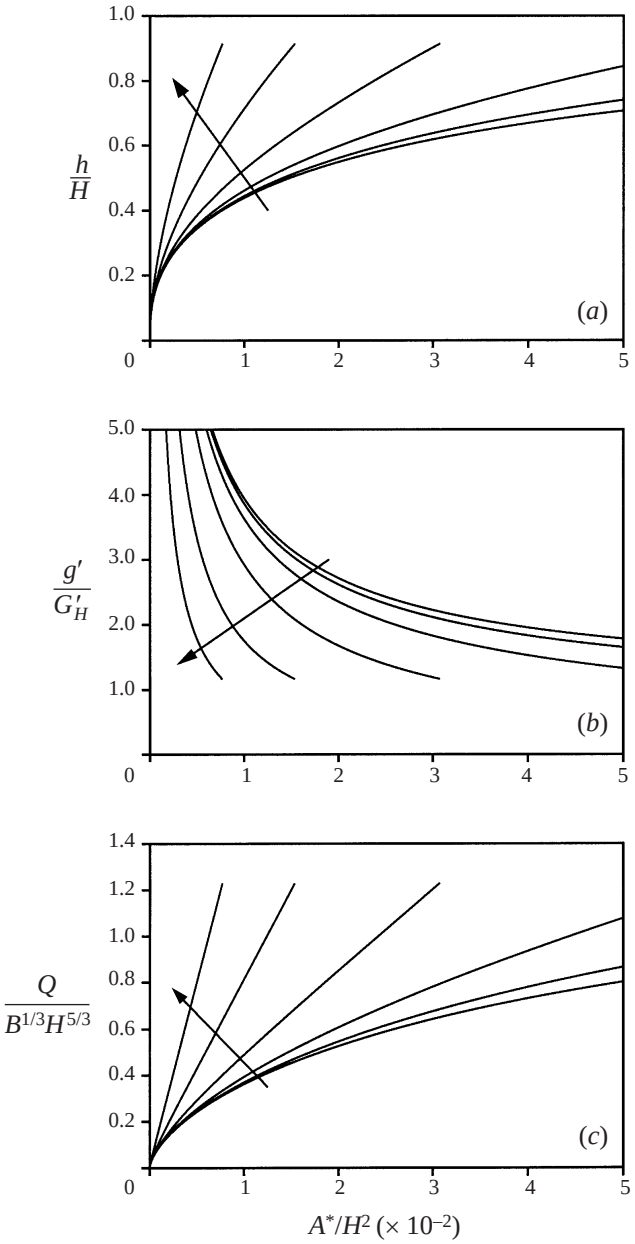

FIGURE 2. Theoretical predictions of displacement flows driven by a point source assisted by wind: (*a*) h/H, (*b*) g'/G'_H and (*c*) $Q/(B^{1/3}H^{5/3})$, vs. A^*/H^2 for $Fr = \{0, 1, 2, 4, 8, 16\}$. The arrow indicates the direction of increasing Fr.

in the buoyancy-induced flow Q_B through the enclosure, see (4*b*). The coordinates of the points at which the curves end in figure 2 correspond to the conditions which result in the interface reaching the bottom of the upper opening.

A striking feature of these results is the change in the form of the dependence of the interface height h/H with the area of openings at high and low Froude numbers (figure 2*a*). At low Fr, the dependence of h or A^* is weak for $A^*/H^2 \gtrsim 0.02$, because a

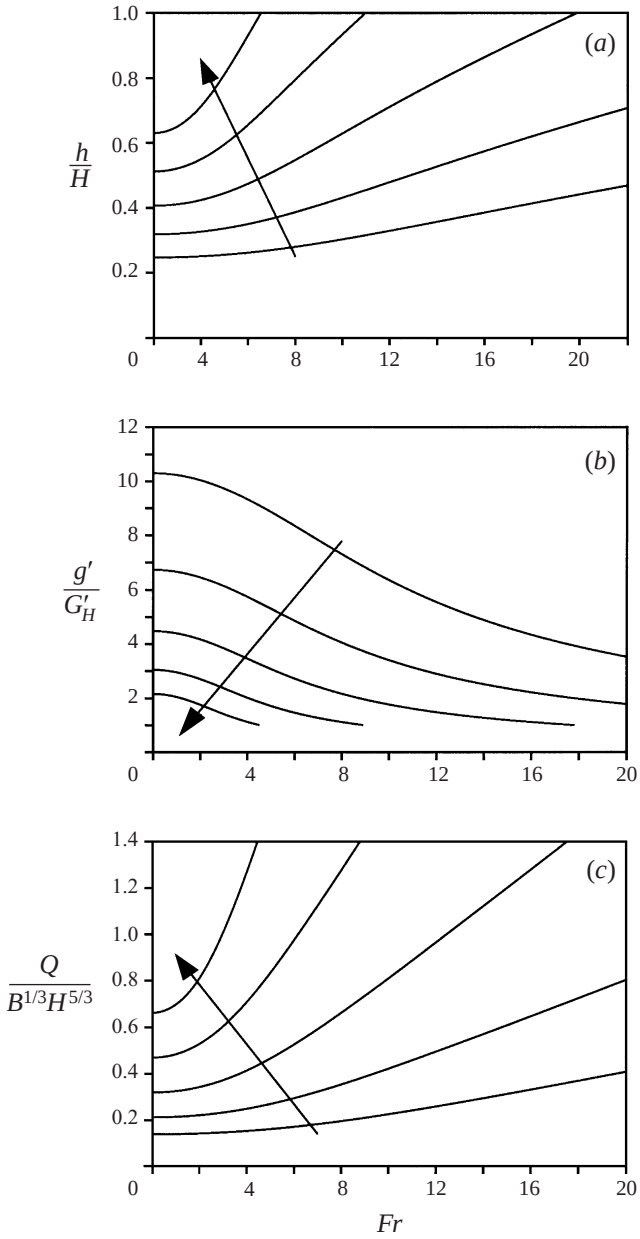

FIGURE 3. Theoretical predictions of displacement flows driven by a point source assisted by wind: (*a*) h/H, (*b*) g'/G'_H and (*c*) $Q/(B^{1/3}H^{5/3})$, vs. Fr for $A^*/H^2 = \{2 \times 10^{-3}, 4 \times 10^{-3}, 8 \times 10^{-3}, 1.6 \times 10^{-2}, 3.2 \times 10^{-2}\}$. The values of A^*/H^2 considered represent successive factor of two increases in area of the openings. The arrow indicates the direction of increasing A^*/H^2.

significant depth of the warm upper layer is required to produce the stack-driven flow. At high Fr, there remains a strong dependence (almost linear) of h and A^*, because the wind is increasingly effective as the openings are enlarged. Of course, on windy days there is a natural tendency to close openings so this effect may not always be realized in practice. Similar trends can be seen in the results shown in figures 3 and 4.

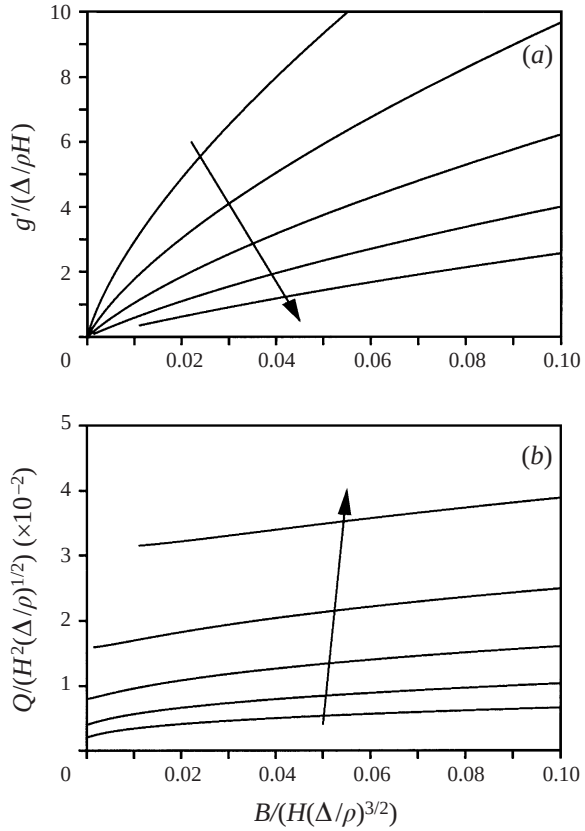

FIGURE 4. Theoretical predictions of displacement flows driven by a point source assisted by wind: (*a*) $g'/(\Delta/\rho H)$ and (*b*) $Q/(H^2(\Delta/\rho)^{1/2})$ vs. $B/(H(\Delta/\rho)^{3/2})$ for $A^*/H^2 = \{2\times10^{-3}, 4\times10^{-3}, 8\times10^{-3}, 1.6\times10^{-2}, 3.2\times10^{-2}\}$. The arrow indicates the direction of increasing A^*/H^2.

Plots of (*a*) h/H, (*b*) g'/G'_H and (*c*) $Q/(B^{1/3}H^{5/3})$ as functions of Fr for $A^*/H^2 = \{2\times10^{-3}, 4\times10^{-3}, 8\times10^{-3}, 1.6\times10^{-2}, 3.2\times10^{-2}\}$ are given in figure 3. Each successive value of A^*/H^2 considered represents a factor of two increase in the opening area A^*. Figure 3(*a*) shows that for a fixed value of Fr the interface height rises as the dimensionless area of the openings is increased. As a consequence, the reduced gravity (figure 3*b*) of the buoyant upper layer decreases and the volume flux through the space (figure 3*c*) increases.

The effect of varying the buoyancy flux B on g' of the upper layer and volume flux Q is shown in figure 4; (*a*) $g'/\Delta/\rho H$ vs. $B/H(\Delta/\rho)^{3/2}$ and (*b*) $Q/(H^2(\Delta/\rho)^{1/2})$ vs. $B/H(\Delta/\rho)^{3/2}$. On increasing B, the ratio between the wind-driven and buoyancy-driven velocities decreases and the height of the interface decreases and approaches the value established in the absence of wind (figure 3*a*). The reduced gravity G' in the plume at the level of the original interface increases and consequently, as the reduced gravity of the upper layer equals that in the plume at the level of the interface in the steady state, the reduced gravity of the upper layer increases (figure 4*a*). Furthermore, as the interface falls and the depth of the buoyant upper layer increases, the buoyancy-driven flow (see (4*b*)), and thus the total volume flow rate through the space increases (figure 4*b*). It should be noted, however, that the volume flow rate, and hence the interface position (see § 4, figure 13*b*) are weak functions of the source strength, because $Q \propto B^{1/3}$.

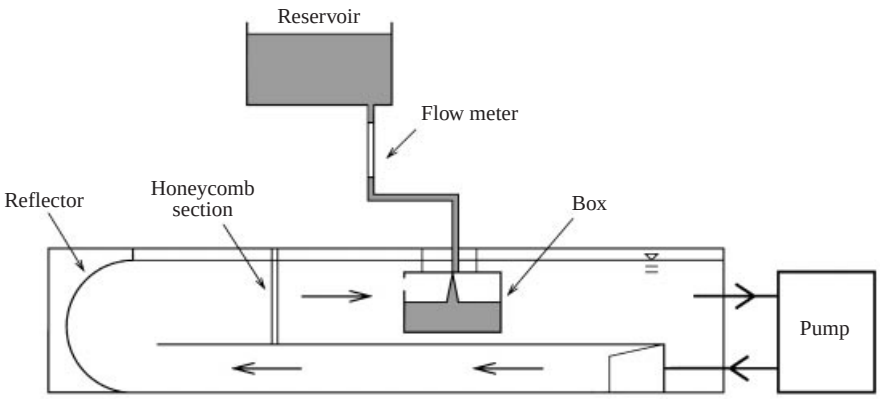

FIGURE 5. A schematic diagram showing the experimental set-up. The flume generated a flow which recirculated in a vertical path. Before reaching the test section the flow was turned by a reflector and passed through a honeycomb gauze in order to give a more uniform velocity profile.

3. Experiments

Experiments were conducted in a Perspex box suspended in the test section of a flume tank (length 2.65 m × width 0.30 m × depth 0.57 m) containing fresh water. The experimental set-up is shown in figure 5. The Perspex box was of constant cross-section (internal dimensions 29.5 cm by 15 cm), 25 cm high, and had a number of circular openings, each of diameter 2 cm, in both the windward and leeward faces at high and low levels. The total area of the openings was varied by removing plastic plugs from these holes.

Stack-driven flows were simulated in the laboratory using brine and fresh water to create density differences and, therefore, the buoyancy forces act downwards in contrast to the orientation assumed in the theory given in § 2. For the Boussinesq flows of concern here, this reversal of the direction of the buoyancy force is unimportant to the dynamics, apart from reversing the sense of the motion. Brine was introduced through a circular nozzle (diameter $D = 0.5$ cm) located at the centre of the top face of the box. Dense fluid was supplied to the nozzle via a constant-head gravity feed and the flow rate was regulated using an in-line flow meter. The nozzle (figure 6) was designed to produce a turbulent plume at the point of discharge. This was achieved by forcing the salt solution through a narrow opening (0.1 cm in diameter) from which it passed into a larger cylindrical chamber (1 cm in diameter) before finally being discharged from the nozzle through a fine mesh. The principle behind the nozzle relies on the sharp expansion exciting a turbulent flow in the large chamber and, consequently, a turbulent flow at the exit. An indication of how well the nozzle works is shown in figure 7. The measured distance H_m between the exit point of the nozzle and the bottom of the box was 23.2 cm and $d_c = 2$ cm. A sheet of fine gauze (8 cm wide and 15 cm in depth), designed to shield the plume from the inflow, was attached to the inside of the box between the windward openings and the plume nozzle. The gauze sheet slowed, rather than completely blocked, the flow travelling towards the plume and prevented the plume from being significantly deflected from the vertical.

The flume generated a controllable, horizontal flow in the test section that represented a flow of wind around the box. This flow resulted in a dynamic pressure drop Δ between the windward and leeward openings which was measured using a manometer tube. The tube was partially filled with a vegetable oil and the two ends of the tube

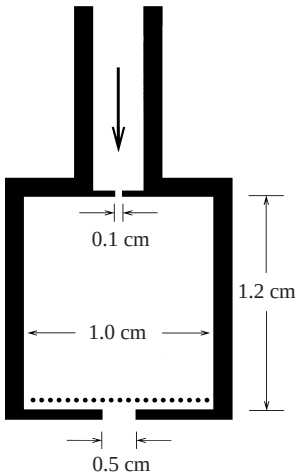

FIGURE 6. Simplified cross-section through the vertical axis of the cylindrical plume nozzle. The nozzle shown (not to scale) is based on a design originally conceived by Dr Paul Cooper of the Faculty of Engineering, University of Wollongong, NSW, Australia. The arrow indicates the direction of flow into the nozzle. The line of dots adjacent to the outlet of the nozzle represent a fine square mesh (aperture size approx. 0.06 cm × 0.06 cm). The diameter (0.5 cm) of the nozzle outlet and the diameter (1 cm) and length (1.2 cm) of the chamber were fixed in the present experiments, although the design of the nozzle allowed these dimensions to be varied.

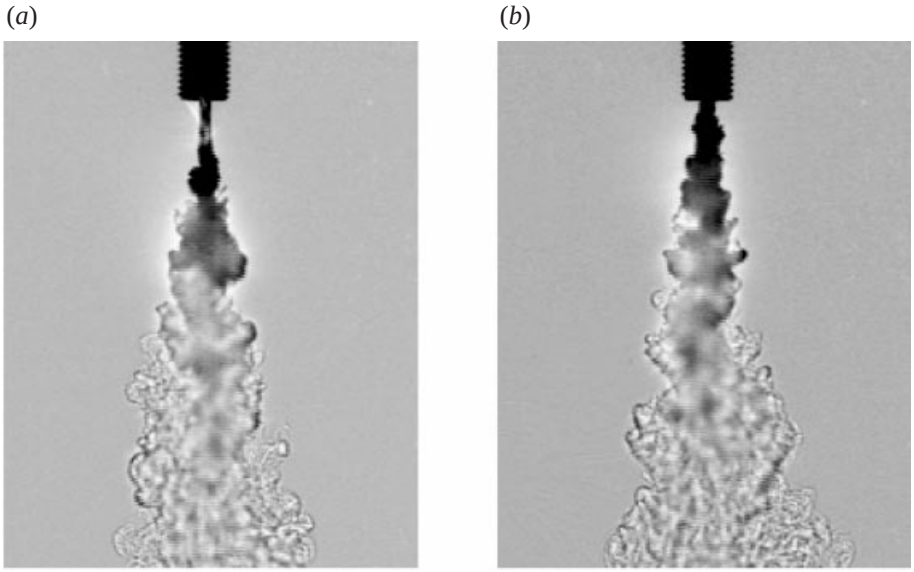

FIGURE 7. Shadowgraph images showing turbulent plumes produced by two different nozzle designs: (*a*) standard nozzle (i.e. a simple cylindrical tube of constant cross-section with a fine mesh at the outlet) and (*b*) nozzle based on Dr Paul Cooper's design (figure 6). In each case the Reynolds number $Re = 220$ is based on the conditions at the source. The vertical distance from the source to the point at which the plume becomes turbulent is approximately 3 source diameters in (*a*) and 1 source diameter in (*b*).

were immersed in the flume and positioned level with and adjacent to the upwind and downwind vents of the box. The displacement of the oil/water interface in the tube was measured for various flow rates in the flume and the resulting 'wind' pressure drop determined (Hunt & Linden 1997). This direct measurement of the pressure

drop meant it was not necessary to determine the mean fluid speed in the flume. Pressure fluctuations of between 5% and 10% of the mean pressure drop were recorded. These fluctuations lead to variations in the Froude number and are represented by horizontal error bars in figure 11. By varying the mean flow speed in the flume (and, hence, the pressure drop across the openings), the opening area and the buoyancy flux of the plume, steady-state flows were examined for a wide range of conditions.

An experiment was started by removing a number of plugs from openings in the box and supplying dense salt solution to the plume. The flume was then started and a 'wind' flow past the box established. When a steady-state flow was established in the box the height of the interface (i.e. the vertical distance between the exit point of the plume nozzle and the interface) was measured using the digital image processing system DigImage (Dalziel 1993). The position of the interface, corresponding to a particular intensity on the digitized images, was tracked during the experiment. The density difference across the interface was determined by extracting bulk samples from the upper and lower layers using a needle syringe and measuring their density using an Anton Paar densitometer. A sample of ambient fluid was extracted in order to account for the (small) background concentration of salt which develops in the flume during the experiments. The assumption that the upper and lower layers were well-mixed was checked by determining detailed density profiles in two cases.

Flows in the box were visualized using two different techniques. The majority were visualized by adding dye to the brine and using a shadowgraph. Images were collected by a video camera and recorded onto video tape. The 'raw' shadowgraph images were enhanced by making a correction for the non-uniform background lighting and then stretching the range of digitized intensities in an image in order to enhance the contrast between regions of mixing in the plume and the surrounding fluid. Experiments to determine density profiles were lit by diffuse back-lighting and, as before, dye was added to the salt solution. By measuring the vertical variation in the light intensity passing through the box, which is attenuated by an amount dependent upon the concentration of the dye, density profiles averaged across the width of the box were inferred. This technique involves a calibration of the camera and of the dye, details of which are given by Cenedese & Dalziel (1998). The light source and the camera were positioned approximately 8.5 m and 2.5 m from the tank, respectively. Parallax errors were estimated at less than 0.1 cm when using a shadowgraph and less than 0.4 cm when back-lighting.

The theoretical description of a turbulent plume by Morton *et al.* (1956) used in § 2 assumes ideal source conditions, i.e. a pure plume from a point source with zero initial fluxes of volume and momentum, and finite buoyancy flux. However, the plumes generated in the experiments issue from an origin (at $x = 0$) of finite area with non-zero initial fluxes of volume Q_{p0}, momentum M_0 and buoyancy B_0. Therefore, before comparing the experimental observations with the theoretical predictions of § 2, a correction (Appendix B) was made to the measured interface height h_m in order to account for the non-ideal source conditions. For the experimental source conditions the correction x_v was typically 0.5–1.5 cm (i.e. of the order of $1D$–$3D$ and significantly less than the height of the box). This correction for the virtual origin is included in the predictions for the interface height by replacing (10) by

$$\frac{A^*}{\hat{H}^2} = \frac{C^{3/2}(\hat{h}/\hat{H})^{5/3}}{((1-\hat{h}/\hat{H}-d_c/\hat{H})/(\hat{h}/\hat{H})^{5/3}+C\hat{F}r^2)^{1/2}}, \tag{20}$$

where the corrected dimensionless height of the interface $\hat{h}/\hat{H}$ and Froude number

$\hat{Fr}$ are

$$\frac{\hat{h}}{\hat{H}} = \frac{h_m + x_v}{H_m + x_v} \quad \text{and} \quad \hat{Fr} = \sqrt{\frac{\Delta/\rho}{(B/\hat{H})^{2/3}}}. \tag{21a,b}$$

The non-dimensional reduced gravity is given by (14) and (16) with $\xi(= h/H)$ and H replaced by $\hat{h}/\hat{H}$ and $\hat{H}$, respectively, so that

$$\frac{g'}{G'_{\hat{H}}} = \left(\frac{\hat{h}}{\hat{H}}\right)^{-5/3} \quad \text{and} \quad \frac{g'}{(\Delta/\rho\hat{H})} = C\hat{Fr}^{-2}\left(\frac{\hat{h}}{\hat{H}}\right)^{-5/3}. \tag{22a,b}$$

For the geometry considered, namely that of the laboratory model, the depth d_c of the 'dead' layer near the ceiling is small relative to the height of the space and over the range of experiments conducted $d_c/\hat{H} = 8.25 \times 10^{-2} \pm 2\%$. However, in some rooms or buildings the depth of the dead layer may be comparable witht the height of the space, in which case we suggest that the following variables are introduced: $\hat{h} = h + x_v$, $\hat{H} = H + x_v - d_c$.

Before proceeding to investigate the effects of wind on the buoyancy-driven displacement flow we examine the effect of the correction for the non-ideal source and the value of the entrainment coefficient on the predictions of the interface height and reduced gravity. We restrict attention to the case of no wind as this allows us to make comparisons with previous results which did not include these factors. The observed steady-state interface heights for $\hat{Fr} = 0$ are shown in figure 8(*a*) as a function of $A^*/\hat{H}^2$, and the theoretical predictions (20) with $\alpha_G = 0.083$ are shown as the continuous line. Comparison with figure 12(*a*) of Linden *et al.* (1990) shows that the agreement between the predicted and observed values has improved. An entrainment coefficient of $\alpha_G = 0.083$ was also used in the model of Linden *et al.* (1990), but without a correction for the non-ideal source. However, it is unclear whether the improved agreement may be attributed entirely to the virtual origin correction ((B 1), see Appendix B) as it may result, at least in part, from the superior plume nozzle design (figure 6) which results in an earlier transition to turbulence (figure 7). Furthermore, the differences in the location of the inlet openings (positioned on the top face in the experiments of Linden *et al.* (1990) and on a side face in the present experiments) and, consequently, in the direction of the inflow may also affect the plume dynamics. In our experiments, the inflowing current is perpendicular to the direction of the plume and, as mentioned earlier, it was necessary to reduce its momentum using a gauze baffle. In contrast, the inflow of Linden *et al.* (1990) was parallel to and co-flowing with the plume.

The sensitivity of the theoretical predictions (20) to the value of the entrainment coefficient is also shown in figure 8(*a*) with $\alpha_G = 0.074$ (dashed line) and $\alpha_G = 0.094$ (dotted line). The volume flux in a plume increases rapidly with increasing distance from its origin ($Q_p \sim \alpha_G^{4/3} x^{5/3}$), and is sensitive to a small increase in the entrainment rate. Consequently $\hat{h}/\hat{H}$ decreases significantly as α_G increases. The reduced gravity of the upper layer as a fraction of the reduced gravity in the plume at the top of the space is plotted against the dimensionless area of openings in figure 8(*b*). The predicted values of (22*a*) are shown for $\alpha_G = 0.083$ (continuous line), $\alpha_G = 0.074$ (dashed line) and $\alpha_G = 0.094$ (dotted line). The sensitivity of the predictions to α_G is clear and the differences between predictions for $\alpha_G = 0.074$ and $\alpha_G = 0.094$ exceed the spread of the data. This test of the theory with two independent measurements,

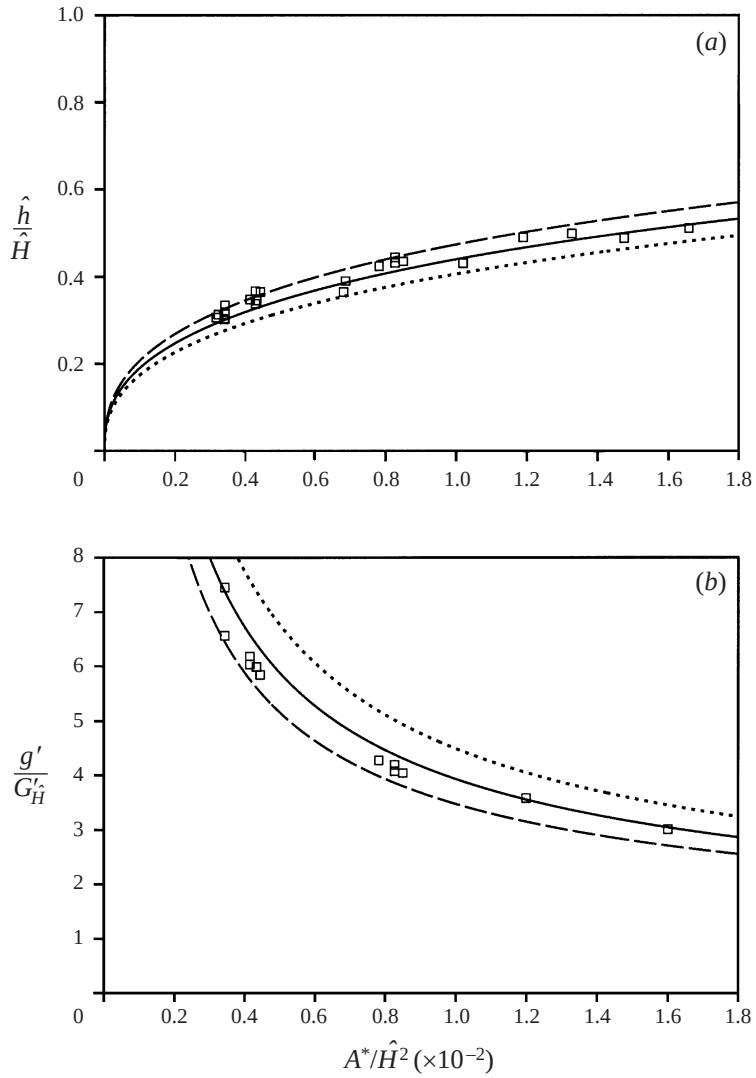

FIGURE 8. Displacement flow driven by a point source of buoyancy $\hat{F}r = 0$. (*a*) The depth $\hat{h}/\hat{H}$ of the zone at ambient density and (*b*) the reduced gravity $g'/G'_{\hat{H}}$ of the buoyant layer as functions of the dimensionless area of the openings $A^*/\hat{H}^2$. The theoretical predictions of equation (20) with $d_c/\hat{H} = 8.25 \times 10^{-2}$ and (22*a*) are shown for $\alpha_G = 0.083$ (continuous line), $\alpha_G = 0.074$ (dashed line) and $\alpha_G = 0.094$ (dotted line).

i.e. of interface height and reduced gravity, suggests that $\alpha_G = 0.083$ is best. During the present experiments, one of the key findings of Linden *et al.* (1990), namely, that in the absence of wind the steady interface heights are independent of the buoyancy flux from the source, was confirmed – these results are not shown.

4. Results

Three sets of experiments with combined wind and buoyancy-driven ventilation, referred to hereafter as EXP1, EXP2 and EXP3, were conducted. EXP1 examined the

effect of the wind pressure drop Δ on the steady-state stratification profiles in the box. The effect of the opening area A^*/H^2 was investigated in EXP2, and finally, in EXP3 the effect of the strength B of the source on the flow in the enclosure was examined.

4.1. *Experiment* EXP1

Once a steady-state displacement flow was established in the box, the flume was switched on and the required 'wind' speed selected. Inflow of ambient fluid was through the high-level, windward openings and the outflow of dense salt solution was through the low-level, leeward openings. A transitory stage followed in which the interface was displaced downwards. During this period the depth and density of the lower layer decreased and, since no fluid crossed the stable interface except in the plume, equilibrium was re-established when the volume flux across the interface in the plume matched the volume flux through the openings. The depth and density of the saline layer were then both less than in the no-wind case. Dye released near the upper opening showed that ambient fluid in the upper layer crossed the interface by first being entrained into the plume.

The displacement mode of ventilation, characterized by a two-layer stratification, was maintained for a wide range of Froude numbers. Figure 9 shows enhanced shadowgraph images of typical displacement flows driven by: (*a*) buoyancy forces alone and (*b*) buoyancy forces assisted by wind. The corresponding density profiles are shown in figure 10 which confirm that an increase in Δ or Fr decreases the density step across the interface and increases the depth of the ambient layer.

The observed steady-state interface heights $\hat{h}/\hat{H}$ and reduced gravity $g'/G'_{\hat{H}}$ are shown as functions of the Froude number $\hat{F}r$ in figures 11(*a*) and 11(*b*), respectively. From figure 11 we see that increasing Δ, and hence $\hat{F}r$, results in an increase in the depth of the ambient layer (thereby implying an increase in the volume flow rate) and a decrease in the density of the saline layer. The areas of both the windward and leeward openings were then doubled and the experiment repeated. These results are shown by the triangular symbols in figure 11. It can be seen that on increasing the dimensionless opening area from $A^*/\hat{H}^2 = 3.4 \times 10^{-3}$ to $A^*/\hat{H}^2 = 6.8 \times 10^{-3}$ the rate of ascent of the interface increases and the density step across the interface is reduced for each value of $\hat{F}r$ considered. This was also observed to be the case for any further increase in $A^*/\hat{H}^2$. There were wave-like disturbances on the interface, typically 0.2–1.5 cm in amplitude. Increasing either Δ or $A^*/\hat{H}^2$ decreased the density contrast across the interface and, consequently, the amplitude of the disturbances increased. These fluctuations are represented by vertical error bars in figure 11.

The systematic difference between the predicted and observed interface heights is believed to be due primarily to the inflow into the enclosure affecting the plume dynamics. At larger values of $\hat{F}r$ there was significant deflection of the plume from the vertical and the discrepancy between observed and predicted interface heights is probably caused by differences in the entrainment rate between the assumed axisymmetric (§ 2) and the observed deflected plume, since the discrepancy increases as $\hat{F}r$ increases. During trial experiments, in which gauze mesh was not used to diffuse the momentum of the inflow, the plume was strongly deflected from the vertical and interface heights were significantly lower than those recorded when the plume was shielded. This implies that the entrainment rate of the deflected plume may be higher than for the undisturbed plume. At present there seems little justification for developing a more complicated model as there is some uncertainty regarding the

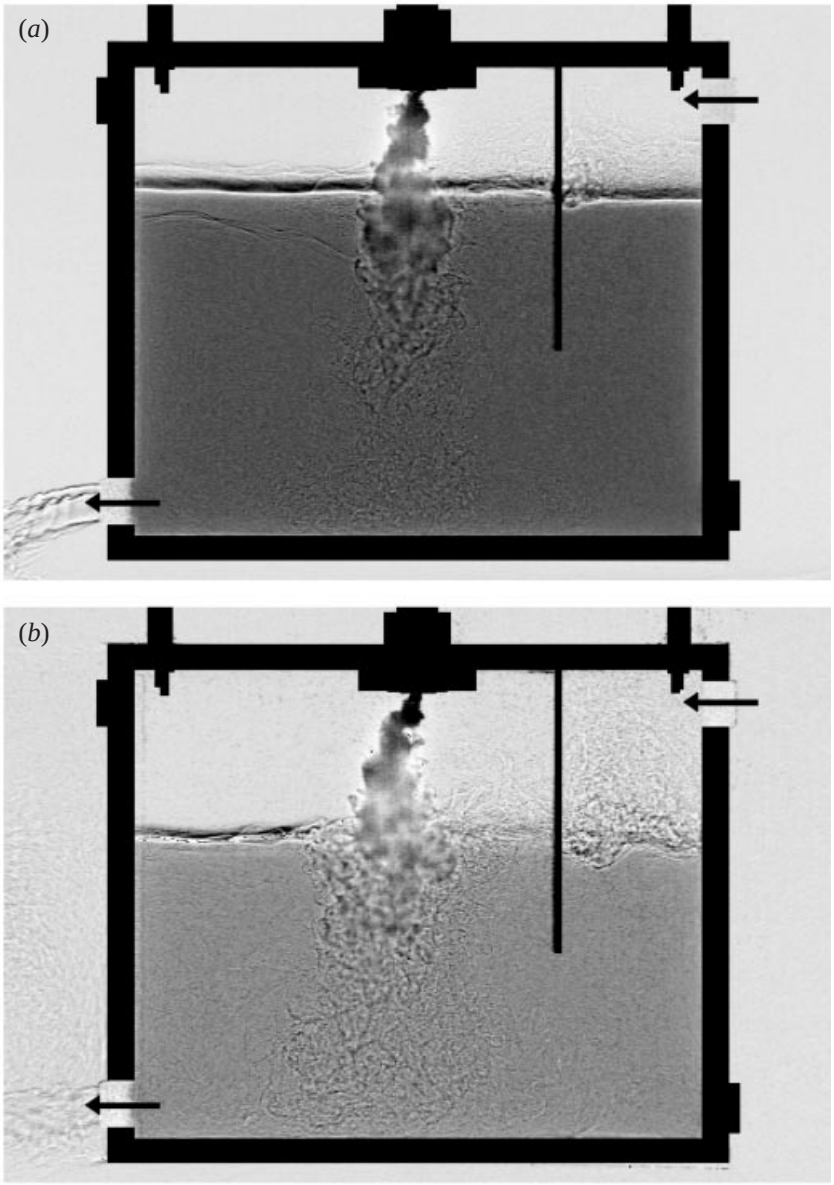

FIGURE 9. Enhanced shadowgraph images showing typical, steady-state displacement flows in an enclosure; (*a*) buoyancy-driven flow $\hat{F}r = 0$, and (*b*) buoyancy-driven flow assisted by wind $\hat{F}r = 9$. The buoyancy flux of the plume $B = 230\,\mathrm{cm^4\,s^{-2}}$, $A^* = 2.03\,\mathrm{cm^2}$, $x_v = 1.3\,\mathrm{cm}$ and the dimensionless area of the openings is $A^*/\hat{H}^2 = 3.4 \times 10^{-3}$. In (*b*) the wind direction is from right to left and $\Delta = 362\,\mathrm{g\,cm^{-1}\,s^{-2}}$ giving $\hat{F}r = 9$. In both cases inflow of ambient fluid is through the upper opening (top right) and outflow of saline solution is through the lower opening (bottom left) as indicated by the arrows. The gauze sheet designed to deflect the inflow from the plume is visible as a vertical line extending from the top to approximately two thirds of the way down the box. The change in the shade of grey in the image, from dark grey in (*a*) to light grey in (*b*), is indicative of a reduction in density.

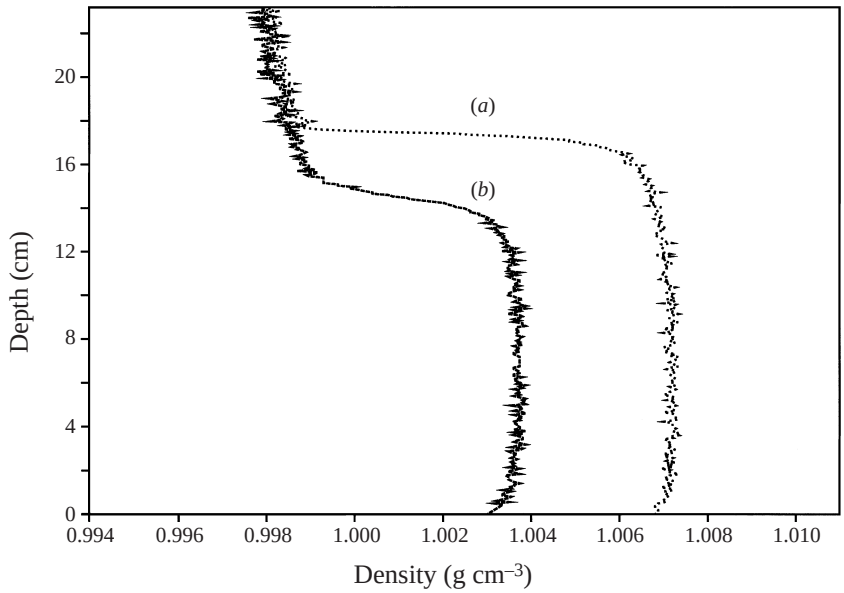

FIGURE 10. Density profiles of typical steady-state, displacement flows driven by (*a*) buoyancy forces alone (note the interface at approximately 17 cm) and (*b*) buoyancy forces assisted by wind (note the interface at approximately 15 cm). The density contrast between the upper and lower layers is significantly reduced in (*b*). The profiles are taken from an experiment with identical conditions to those described in figure 9, and were determined by introducing a coloured dye to the lower layer via the plume and measuring the attenuation of the light which passed through the dye; the amount by which the light was attenuated is directly proportional to the dye concentration, and hence, the fluid density.

appropriate value for the entrainment coefficient for deflected plumes and, in practice, this effect is likely to be minimal because ventilation systems are usually designed to reduce draughts. A second effect which acts to reduce the observed interface height is mixing at the interface caused by the inflow of 'wind'. In the present experiments interfacial mixing was relatively small and this effect was slight.

Experiment EXP1 was then repeated, this time measuring the interface height and density contrast as the wind pressure drop was decreased, rather than increased. The results obtained for decreasing Δ were observed to be indentical to those which were established as Δ was increased, i.e. no hysteresis effects were observed. Again EXP1 was repeated, but this time, however, the experiment was started by first establishing a 'wind' flow in the flume and then supplying fluid to the plume. Again the results were found to be indentical to those of EXP1.

4.2. *Experiment* EXP2

In these experiments, wind-assisted displacement flows were examined for a wide range of opening areas. B and Δ were fixed and the position of the interface and the lower-layer reduced gravity were measured once a steady-state flow was established. The area of the openings was then changed and measurements taken once steady-state flow conditions were reached. The effect of the dimensionless opening area on the stratification is shown in figure 12 where (*a*) $\hat{h}/\hat{H}$ and (*b*) $g'/G'_{\hat{H}}$ are plotted against $A^*/\hat{H}^2$. It is observed, as predicted, that $\hat{h}/\hat{H}$ increases and $g'/G'_{\hat{H}}$ decreases as $A^*/\hat{H}^2$ increases. This increase in the ambient-layer depth implies an increase in the volume flux through the space.

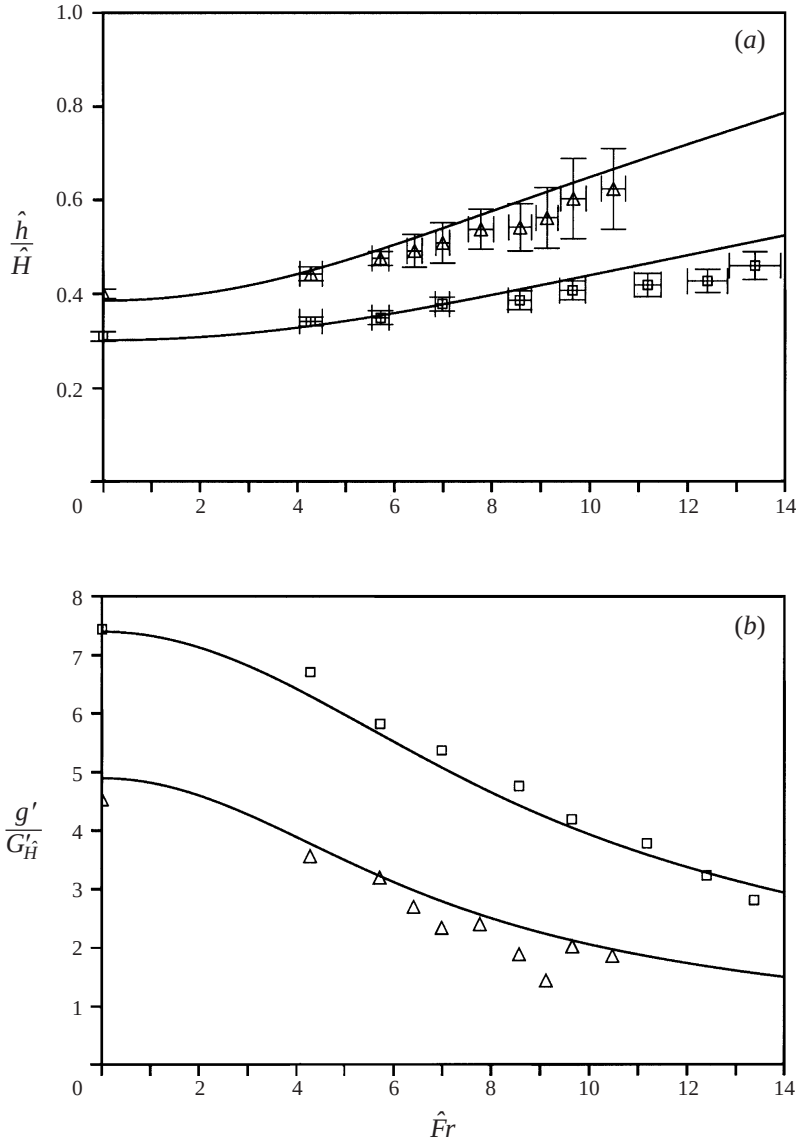

FIGURE 11. Effect of wind speed: displacement flow driven by a point source assisted by wind. $\hat{Fr}$ was increased during the experiments by increasing Δ. (*a*) $\hat{h}/\hat{H}$ and (*b*) $g'/G'_{\hat{H}}$ vs. $\hat{Fr}$. The square symbols show results for $A^*/\hat{H}^2 = 3.4 \times 10^{-3}$ and the triangular symbols for $A^*/\hat{H}^2 = 6.8 \times 10^{-3}$. In both cases $B = 192\,\mathrm{cm^4\,s^{-3}}$, $G'(x = 0, B) = 140.6\,\mathrm{cm\,s^{-2}}$ and $x_v = 1.2\,\mathrm{cm}$. The theoretical predictions of (20) and (22*a*) are shown by the continuous curves.

4.3. *Experiment* EXP3

Finally, a series of experiments was conducted to examine the effect of B on the stratification profiles within the box. During these experiments $A^*/\hat{H}^2$ and Δ were fixed, and B was increased either by increasing the initial volume flow rate $Q_p(x = 0, B)$ or the initial reduced gravity $G'(x = 0, B)$ of the plume. A steady-state flow driven by a plume of buoyancy flux B_1 was first established and then the buoyancy flux of the plume was changed to B_2 and the properties of the resulting steady state measured.

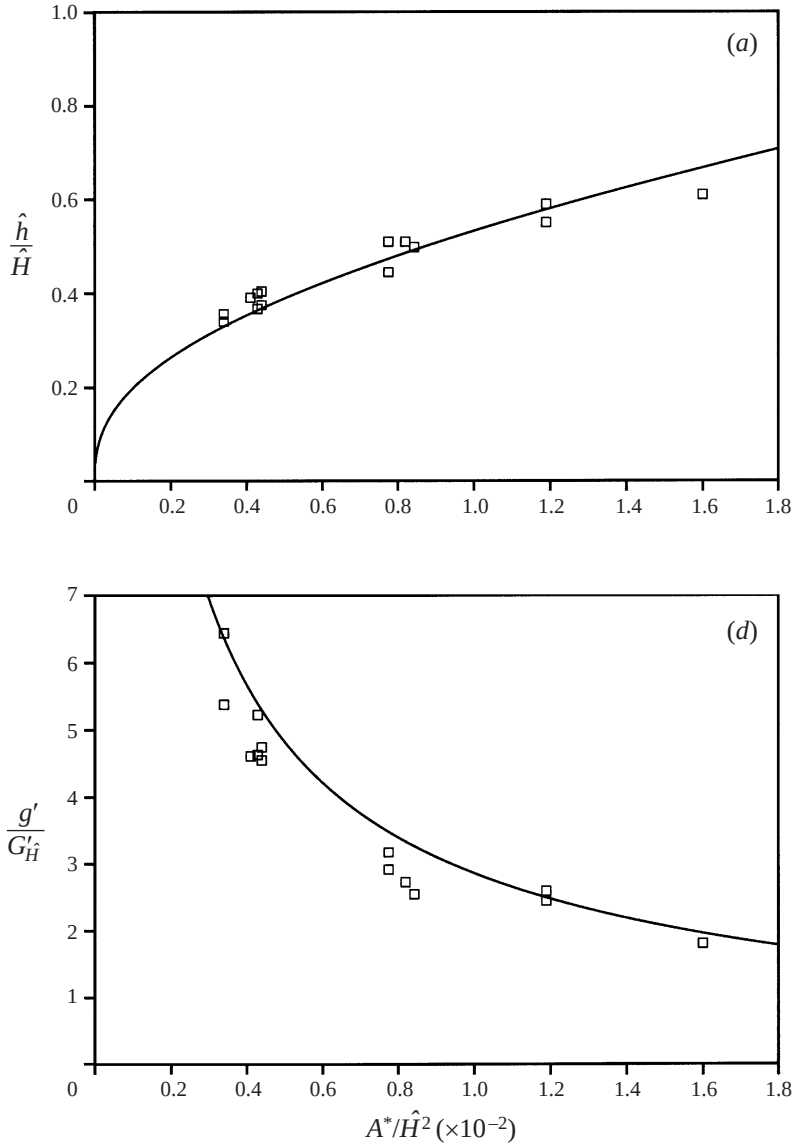

FIGURE 12. Effect of opening area: displacement flow driven by a point source assisted by wind: (*a*) $\hat{h}/\hat{H}$ and (*b*) $g'/G'_{\hat{H}}$ vs. $A^*/\hat{H}^2$. The quantities used in the experiment shown were $G'(x=0,B)=143\,\mathrm{cm\,s^{-2}}$, $B=207.5\,\mathrm{cm^4\,s^{-3}}$ and $\Delta=72\,\mathrm{g\,cm^{-1}\,s^{-2}}$ giving $\hat{F}r=4.2$ ($x_v=1.3\,\mathrm{cm}$). The theoretical predictions of (20) and (22*a*) are shown by the continuous curves.

Figures 13(*a*) and 13(*b*) show $\hat{h}/\hat{H}$ plotted against the dimensionless source strength $B/(\hat{H}(\Delta/\rho)^{3/2})$ and the Froude number $\hat{F}r$, respectively. The dimensionless reduced gravity $g'/(\Delta/\rho\hat{H})$ of the lower layer is plotted as a function of $B/(\hat{H}(\Delta/\rho)^{3/2})$ in figure 13(*c*). The interface height is a weak function of the source strength (figure 13*a*), although the density step across the interface is strongly dependent upon the source strength (figure 13*c*); a factor of four increase in $B/(\hat{H}(\Delta/\rho)^{3/2})$ from 0.5×10^{-2} to 2×10^{-2} results in less than a 5% decrease in $\hat{h}/\hat{H}$ and over a three-fold increase in $g'/(\Delta/\rho\hat{H})$.

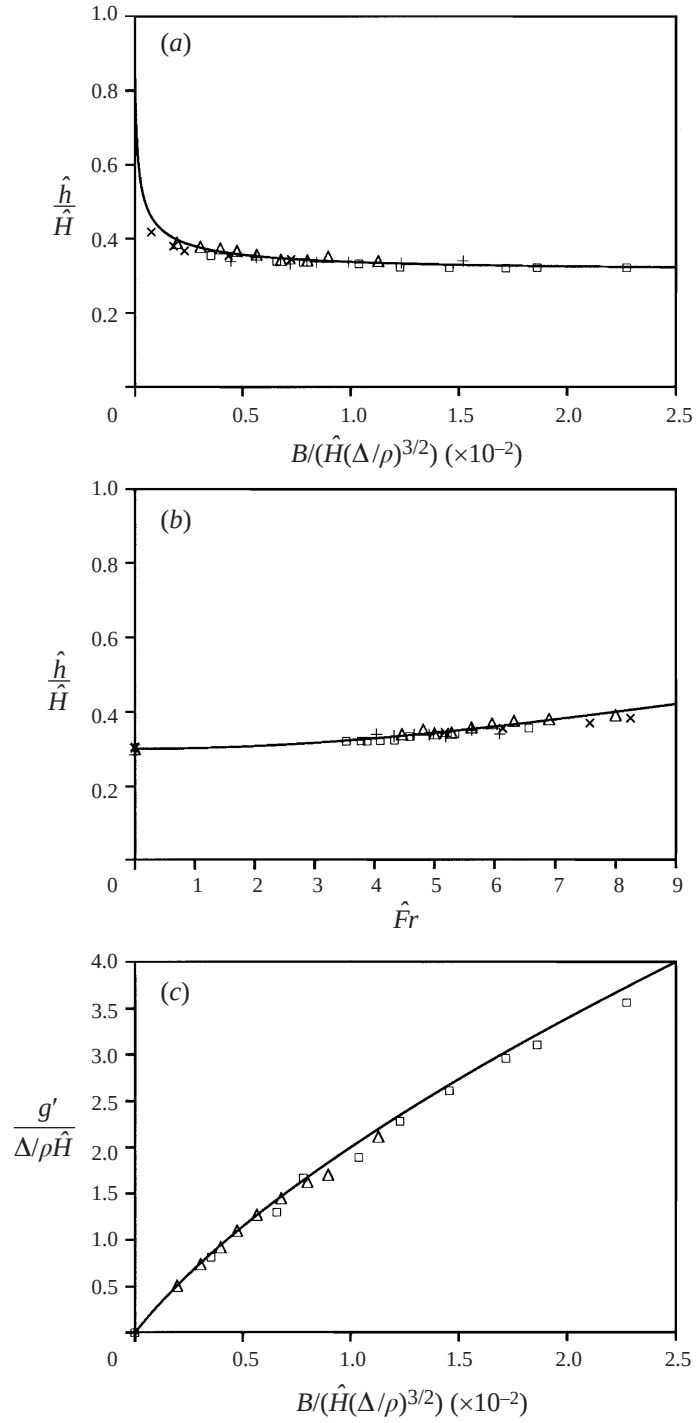

FIGURE 13. Effect of source strength: displacement flow driven by a point source assisted by wind: (*a*) $\hat{h}/\hat{H}$ vs. $B/\hat{H}(\Delta/\rho)^{3/2}$, (*b*) $\hat{h}/\hat{H}$ vs. $\hat{Fr}$ and (*c*) $g'/G'_{\hat{H}}$ vs. $B/\hat{H}(\Delta/\rho)^{3/2}$. The theoretical predictions of (20) and (22*b*) are shown by the continuous curves. $A^* = 2.03\,\mathrm{cm}^2$, $H_m = 23.2\,\mathrm{cm}$, x_v varied between 0.64 and 1.54 cm. $A^*/\hat{H}^2 \approx 3.4 \times 10^{-3} \pm 5\%$. $\times$, $G'(x = 0, B) = 51\,\mathrm{cm\,s^{-2}}, \Delta = 72\,\mathrm{g\,cm^{-1}\,s^{-2}}$; $+$, $G'(x = 0, B) = 97\,\mathrm{cm\,s^{-2}}, \Delta = 72\,\mathrm{g\,cm^{-1}\,s^{-2}}$; $\triangle$, $G'(x = 0, B) = 157\,\mathrm{cm\,s^{-2}}, \Delta = 72\,\mathrm{g\,cm^{-1}\,s^{-2}}$; $\square$, $G'(x = 0, B) = 183\,\mathrm{cm\,s^{-2}}, \Delta = 123\,\mathrm{g\,cm^{-1}\,s^{-2}}$.

Increasing the source strength decreases the depth of the ambient layer while increasing the depth and density of the driving lower layer. The buoyancy-driven flow rate, see (4*b*), and, consequently, the total flow rate are thereby enhanced. An increase in the source strength corresponds to a decrease in $\hat{Fr}$ (see (11)) and as expected the depth of the ambient layer was observed to decrease slightly (figure 13*b*). We recall from EXP2 that reducing $\hat{Fr}$ by decreasing Δ decreased the volume flux through the enclosure. The data points shown in figure 13 represent measurements taken from a number of separate experiments each with different initial reduced gravities. Two 'wind' speeds, corresponding to $\Delta = 72\,\mathrm{g\,cm^{-1}\,s^{-2}}$ and $\Delta = 123\,\mathrm{g\,cm^{-1}\,s^{-2}}$, were considered. In figure 13(*a–c*) the data have collapsed onto a single curve thus confirming the scalings.

4.4. *Breakdown of the displacement flow*

We observe that displacement flow and two-layer stratification are maintained for a wide range of Froude numbers, and buoyancy effects set the flow pattern in the interior even when the wind-produced velocities are relatively large compared with the buoyancy-produced velocities (figure 9). However, it might be expected that there is a critical Froude number above which the wind-induced velocities are so large that it is no longer possible to maintain a displacement flow.

A partial breakdown of the displacement mode of ventilation was observed in the experiments and occurred due to the deflection of the plume resulting from the inflow through the upper openings. In order to counteract this effect, a vertical perforated plate was mounted inside the box (as described in § 3) which diffused the horizontal momentum of the inflow and deflected flow away from the plume. In the absence of this plate, the plume was significantly deflected from the vertical even under the conditions of no wind. It was observed that the depth of the layer at ambient density generated by a deflected plume in a cross-flow was significantly less than for a plume in quiescent surroundings, thus implying an increased entrainment by the deflected plumes. Using a non-perforated plate the plume was well shielded although the inflow was then deflected vertically and a partial breakdown of the displacement flow occured as this current broke through the fluid interface, creating an 'overturning' motion and mixing. The size of the perforations was adjusted in an attempt to maximize the effectiveness of the plate in reducing the horizontal momentum of the inflow while minimizing the vertical deflection of this current. This resulted in a partial breakdown for $\hat{Fr} \approx 20$ (when $A^*/\hat{H}^2 = 3.4 \times 10^{-3}$).

Using the present apparatus it was not possible to cause a complete breakdown of the displacement flow and the Froude number at which a partial breakdown occurred was strongly dependent upon the degree of plume shielding. In building ventilation, fresh air is often channelled into the building at subfloor level and enters the space through grilled openings located on the floor. In addition, these openings are suitably sized and baffled so as to prevent uncomfortable draughts. In this case, the inflow has little horizontal momentum and consequently will not significantly deflect the rising plumes. It is expected that a displacement mode of ventilation will be maintained when adopting this opening arrangement. If the flow through the inlets in the experiments did not deflect the plume we estimate from (19) that the interface will reach the base of the upper openings for $\hat{Fr} \approx 33$ when $A^*/\hat{H}^2 = 3.4 \times 10^{-3}$. This figure is larger than the value $\hat{Fr} \approx 20$ observed, but is of a similar magnitude and the discrepancy is consistent with increased entrainment by a deflected plume.

5. Application to building ventilation

In order to accurately reproduce air flows which occur in naturally ventilated spaces using small-scale models in water tanks, dynamical similarity must be achieved. For stack-driven flows, Baker & Linden (1991) show that dynamical similarity can be achieved as the effects of friction and diffusion can be appropriately scaled when brine is used to create density differences. For steady-state flows driven by the combined effects of stack and wind, the relative magnitudes of the wind- and buoyancy-produced flows are characterized by Fr, and to achieve similarity, Fr must be matched between the experiments and full scale, i.e. we require

$$\frac{(\Delta/\rho)_{\text{model}}}{(\Delta/\rho)_{\text{full-scale}}}\left(\frac{H_{\text{model}}}{H_{\text{full-scale}}}\right)^{2/3}\left(\frac{B_{\text{full-scale}}}{B_{\text{model}}}\right)^{2/3}=1. \tag{23}$$

Models of rooms or buildings used in the laboratory experiments are typically 1/20th–1/100th of full scale, and hence, $H_{\text{model}}/H_{\text{full-scale}} \sim 0.05$–$0.01$. Heat fluxes from individual sources in domestic buildings are likely to be in the range 1 W to 1 kW which is equivalent to buoyancy fluxes of between 2.75×10^{-5} and $2.75\times10^{-2}\,\text{m}^4\,\text{s}^{-3}$ in air at 15°C. These compare with typical buoyancy fluxes of 10^{-7}–$10^{-5}\,\text{m}^4\,\text{s}^{-3}$ for saline plumes in the laboratory (based on $Q_p(x=0,B)\sim O(1)$–$O(10)\,\text{cm}^3\,\text{s}^{-1}$ and $G'(x=0,B)\sim O(10)$–$O(10^2)\,\text{cm}\,\text{s}^{-2}$), and hence, $B_{\text{full-scale}}/B_{\text{model}}\sim O(10^2)$–$O(10^3)$. In the UK, wind speeds are generally less than $10\,\text{m}\,\text{s}^{-1}$ with the average wind speed usually taken to be $4\,\text{m}\,\text{s}^{-1}$ for ventilation design purposes. This range of wind speeds results in $\Delta_{\text{full-scale}}$ up to $O(10^2)\,\text{kg}\,\text{m}^{-1}\,\text{s}^{-2}$. The flume tank described in § 3 was capable of producing a maximum mean flow velocity of approximately $0.2\,\text{m}\,\text{s}^{-1}$ and 'wind' pressure drops in the range $\Delta_{\text{model}}\sim O(1)$–$O(10^2)\,\text{kg}\,\text{m}^{-1}\,\text{s}^{-2}$ were measured. In a building 10 m tall these quantities imply Fr of up to $O(100)$. Using the present experimental apparatus it was possible to examine flows in the range $0\leqslant Fr<20$, the upper limit of 20 being set by the maximum wind speed attainable in the flume and the minimum buoyancy flux (approximately $60\,\text{cm}^4\,\text{s}^{-3}$) required to produce a turbulent plume at the nozzle exit.

The theory and experiments described in § 2–4, therefore, provide a means of predicting air movement and stratification profiles within full-scale buildings when the flow is driven by both the wind and the buoyancy forces. Although the theory of § 2 provides useful insight into the parameters controlling wind-assisted displacement ventilation, there are limitations imposed on its range of applicability due to the underlying assumptions. We assumed that heat gains may be represented as a point source (or point sources) of buoyancy on the floor of the space and that heat transfers between the building fabric and the air in the interior are negligibly small. Linden *et al.* (1990) have shown how this simple approach can lead to an improved understanding of building ventilation. In some circumstances, however, this approach may represent an oversimplification. For example, numerous heat sources may lead to the possibility of plume–plume interactions (Kaye 1998), more complex stratifications (Cooper & Linden 1996), or if the heat source occupies a significant fraction of the floor area it may be more accurately represented as a distributed source. As we have observed, mixing may occur at the interface due to inflow through openings and this will tend to lower the interface position. In fact, if the heat source is weak or if the opening areas are increased, on a windy day the stratification may be destroyed and the model will no longer apply. This breakdown of the stratification and the resulting mixing flow is considered in a related paper Hunt & Linden (2001).

The simplifying assumptions made in § 2 also implicitly impose geometrical restrictions which limit the validity of the model. In § 2 the pressure drop driving the flow through an opening is taken to be that at the mid-height of the opening. The model may therefore be applied only to enclosures for which the vertical extent of the openings is relatively small compared with the overall height of the space (so that the variation in pressure between the top and bottom of the opening is small compared with the variation in pressure between the top and bottom of the space). This may not always be the case in practice. No restriction is placed explicitly on the aspect ratio of the enclosure for which the steady flow model is valid, other than to allow the plume to rise unhindered and entrain freely. For a cylindrical enclosure of radius R, a crude estimate of the maximum aspect ratio H/R for which the rising plume is unhindered may be obtained by considering the vertical distance above the source at which the plume radius equals the radius of the enclosure. The plume radius $b = 6\alpha x/5$ (Morton *et al.* 1956) and, hence, we shall take the maximum aspect ratio for which the model applies to be

$$\frac{H}{R} = \frac{5}{6\alpha} \simeq 7. \tag{24}$$

Clearly, for $H/R \gtrsim 7$ the plume is likely to reach the sidewalls before the ceiling and the classical model for entrainment may no longer hold. This is unlikely to be a serious restriction in practice.

In building ventilation, a fundamental problem confronted by architects and engineers at the design stage is to determine the location and area of openings that will provide the necessary ventilation. This is known as the 'inverse problem' as rather than calculating the air flow rate based on a given area of openings, an openable area is sought which will ensure a specified air flow. This task is further complicated as the comfort of occupants must also be considered when addressing this problem. A sensible strategy is to size the inlet and outlet openings so that their effective area and location ensures that both (i) the air flow provides the necessary cooling over the range of wind speeds and internal heat gains expected and (ii) the height of the stratification is well above the occupied zone.

By locating the openings so that wind assists the buoyancy-driven flow the ventilation rate may be significantly enhanced. In order to maintain a displacement flow, the windward openings should be located at low level and in regions of positive wind pressure, and the leeward openings at high level in regions of negative wind pressure. The 'leeward' openings need not necessarily lie on the leeward face of the building but could instead be positioned in regions of flow separation, e.g. on a flat or pitched roof or on the sidewalls of the building. By locating the openings in regions of extreme positive and negative wind pressures the wind-induced contribution to the air flow may be maximized. Tables of wind pressure coefficients and diagrams indicating regions of positive and negative wind pressures on buildings of different geometries and for varying wind directions and exposure levels are given by Orme, Liddament & Wilson (1994). Wind pressure coefficients relate the surface pressure on the building to the stagnation pressure, and hence, the pressure coefficients at the inlet and outlet openings may be written

$$C_{pi} = P_{wi}/(\tfrac{1}{2}\rho U_{\text{wind}}^2) \quad \text{and} \quad C_{po} = P_{wo}/(\tfrac{1}{2}\rho U_{\text{wind}}^2), \tag{25a, b}$$

where P_{wi} and P_{wo} denote the surface pressures at the respective openings and U_{wind} denotes the mean wind speed. By combining (25*a*) and (25*b*) we can relate the wind

pressure drop Δ to the wind speed:

$$\Delta = \tfrac{1}{2}\rho U_{\text{wind}}^2 (C_{pi} - C_{po}). \tag{26}$$

For typical rectangular buildings on exposed sites the pressure coefficients assume approximately constant values over almost the entire windward and leeward faces, the exception being near the corners (Orme *et al.* 1994). Consequently, the low-level openings may be located on the windward façade at any position below the level of the interface without significantly affecting the driving produced by the wind. The leeward openings, however, should be located as high as possible so as to maximize the driving produced by the buoyant layer of air. If there are non-unidirectional winds (i.e. no prevailing wind direction), locating openings to provide effective ventilation is a far more complex problem. As mentioned earlier, the roof of a building is nominally a region of negative wind pressure irrespective of wind direction (at least for exposed locations) so openings here will act as outlets. A possible solution for the location of the lower openings is a sheltered location which ensures positive wind pressures relative to the upper openings. In cities, or other 'built-up' urban environments, the wind pressure distribution on the building envelope is likely to be more complicated than that on exposed sites, and wind tunnel testing may be necessary to determine suitable locations for openings. Modern naturally ventilated buildings may be equipped with weather stations, for monitoring wind speed and direction, and electronic management systems which respond to weather changes and internal conditions by opening or closing vents accordingly.

We now examine the steady-state temperature distribution within a naturally ventilated space. The convective power E (in W) of a heat source can be converted into a buoyancy flux using

$$B = \frac{g\beta E}{\rho c_p}, \tag{27}$$

where c_p is the specific heat of the air and β is the coefficient of thermal expansion. Substituting for (26) and (27) into (11), the Froude number may be expressed as

$$Fr = U_{\text{wind}} \left(\frac{C_{pi} - C_{po}}{2} \right)^{1/2} \left(\frac{H\rho c_p}{g\beta E} \right)^{1/3}, \tag{28}$$

and from (10) the height h of the interface separating the warm and cool layers of air can now be estimated (or conversely, A^* estimated by specifying the required h). The volume flux through the enclosure (13) is then given by

$$Q = C \left(\frac{g\beta E}{\rho c_p} \right)^{1/3} h^{5/3}. \tag{29}$$

Ventilation rates in buildings are usually expressed in terms of the number of air changes per hour ACH, and for a space with volume V we have

$$\text{ACH} = 3600 \frac{Q}{V} = 3600 \frac{C}{V} \left(\frac{g\beta E h^5}{\rho c_p} \right)^{1/3} \tag{30}$$

for an interface at a height h. The density step $\Delta\rho$ across the interface can be converted into an equivalent temperature difference using the equation of state, namely, $\Delta\rho/\rho = -\beta(T_u - T_a)$, where T_u and T_a denote the respective temperatures of the warm upper layer and the cool lower layer. Substituting for (27) into (14) and

	Buoyancy-driven ventilation	Buoyancy-driven ventilation assisted by wind		
$U_{\text{wind}}(\text{m s}^{-1})$	0	1	2	4
Fr	0	6	12	24
$A^*(\text{m}^2)$	0.1144	0.1144	0.1144	0.1144
h(m)	2.0	2.18	2.65	3.76
$T_a(^\circ\text{C})$	15.0	15.0	15.0	15.0
$T_u(^\circ\text{C})$	18.7	18.3	17.3	16.3
$Q(\text{m}^3\,\text{s}^{-1})$	0.108	0.125	0.173	0.309
ACH	3.9	4.5	6.2	11.1

TABLE 1. A comparison between steady-state natural ventilation flows driven by buoyancy forces alone and those assisted by wind. The pressure coefficients at the windward inlet and leeward outlet are taken to be $C_{pi} = 0.7$ and $C_{po} = -0.2$, respectively. The physical properties of the ambient air at 15 °C are taken to be $\beta = 3.48 \times 10^{-3}\,^\circ\text{C}^{-1}$, $c_p = 1012\,\text{j kg}^{-1}\,^\circ\text{C}^{-1}$ and $\rho = 1.225\,\text{kg m}^{-3}$ (Batchelor 1967, p. 594). The number of air changes per hour is based on an enclosure of volume $V = 1000\,\text{m}^3$.

eliminating $g'(= g\beta(T_u - T_a))$ yields the temperature of the upper layer, namely

$$T_u = T_a + \frac{1}{g\beta C h^{5/3}} \left(\frac{g\beta E}{\rho c_p} \right)^{2/3}. \tag{31}$$

Quantitative predictions for the steady-state height of the interface, temperature of the upper layer and ventilation rate in a building 10 m tall are shown in table 1. The effective area of the openings has been chosen to produce an interface at a height of 2 m above the floor when the flow through the space is driven solely by a point source of buoyancy of strength 0.5 kW. The vertical distance between the centre of the upper opening and the ceiling $d_c = 1$ m. Predictions of h, T_u, Q and ACH are given in the first column of table 1 for buoyancy-driven flows; the remaining three columns show predictions for buoyancy-driven flows assisted by a wind of speed 1, 2 and $4\,\text{m s}^{-1}$, respectively.

For the example shown, an assisting wind speed of $4\,\text{m s}^{-1}$ results in almost a three-fold increase in the ventilation rate when compared with the flow driven solely by buoyancy forces. In addition, the warm upper layer has been reduced in temperature by over 2 °C and in depth by over 1.75 m. For a cube-shaped enclosure this results in a 188% increase in the area of the building fabric which is exposed to the cooler ambient air. Thus, by harnessing the driving produced by the wind, ventilation for passively cooling the space can be achieved. The reduction in temperature of the 'hot' layer passively cools the building fabric and, in addition, a greater area of the building fabric is exposed to the ambient air (as h has increased) thereby further increasing the potential for cooling.

Once the location of the openings has been selected the air flow rate through the building may then be controlled simply by adjusting the area of the openings. For displacement ventilation, the air flow rate is largely controlled by the opening with the smallest area (e.g. if $a_L \gg a_W$, $A^* \sim (2C_e)^{1/2} a_W$, see (5)). Therefore, as for flows driven solely by buoyancy forces (Linden *et al.* 1990), it is possible to control the buoyancy- and wind-driven flow by a single opening. The problem of overheating resulting from the 'hot' layer increasing in depth and descending to the occupied spaces of the building may be overcome by careful design; openings must be adjustable and of sufficient area to ensure that increases in internal heat gains and

subsequent reductions in interface heights (and increases in upper layer temperatures) may be counteracted by increases in vent area.

The floor to ceiling height is another important dimension to consider in the design of a space, not only in terms of the proposed use of the space but also in terms of achieving the required ventilation. For a given wind speed and source strength, Fr increases as the floor to ceiling height increases (assuming as before that the source is located on the floor). In other words, wind effects are more significant in taller spaces, Furthermore, if the geometric ratio A^*/H^2 is maintained at a constant value as H is increased then the depth of the layer at ambient temperature will increase, implying an increase in the ventilation flow rate and a decrease in the upper-layer temperature. Thus, the potential for cooling may be increased by increasing the floor to ceiling height.

6. Conclusions

In this paper we have examined the steady flow and stratification generated in a ventilated enclosure by a single point source of buoyancy on the floor and a flow of wind which assists the buoyancy-driven flow. Laboratory experiments in water tanks have been conducted in order to study these flows and the results compared with the predictions of a theoretical model.

Natural ventilation flows driven by buoyancy forces assisted by wind show similar but more complex flow characteristics to those driven by buoyancy forces alone. We observe that the displacement flow and two-layer stratification established in the absence of wind is maintained for a wide range of wind speeds. The steady-state height h/H of the interface above the source is determined by entrainment into the plume, the dimensionless area of the openings A^*/H^2 and the Froude number $Fr = (\Delta/\rho)^{1/2}(H/B)^{1/3}$. The Froude number is a measure of the relative strengths of the wind- and buoyancy-produced velocities and is directly proportional to the wind speed; for $Fr \ll 1$ the buoyancy forces dominate the fluid motion while for $Fr \gg 1$ the wind forces are dominant. However, even on a windy day, i.e. for $Fr \gg 1$, the buoyancy, although providing little expelling force, may have a significant effect on the air movement and stratification by setting the flow patterns inside the space.

The interface may be raised by increasing A^*/H^2 or Fr (or both). Increasing A^*/H^2 results in an increase in the volume flow rate driven through the enclosure and a decrease in the density step, or equivalently, the temperature of the upper layer. Quantitatively, increasing the wind speed (and, hence, Fr) has the same effect as increasing A^*/H^2. An increase in the strength B of the source decreases Fr (as $Fr \sim B^{-1/3}$) and reduces the interface height. In this case the volume flow through the openings increases due to an increase in both the depth of the buoyant upper layer and the density contrast across the interface. These results are in contrast to solely buoyancy-driven flows where the position of the interface is independent of B. The steady flows, both under conditions of wind and no wind, have no dependence on the cross-sectional area of the space.

The theoretical model developed in § 2 may be used to estimate the steady-state interface heights, stratification profiles and ventilation flow rates for naturally ventilated enclosures. The steady interface height is determined primarily by entrainment into the rising plume and we have shown that the theoretical predictions are sensitive to the plume entrainment coefficient. A number of simplifying assumptions have been made in the model which restrict the range of practical situations to which it may be successfully applied: (i) the model does not account for interactions between the

thermal mass of the building and the air flow in the interior and (ii) it is assumed that heat sources can be represented by a point source (or equal-strength non-interacting point sources) of buoyancy. Restrictions are also placed on the range of enclosure geometries covered by the simple model. An estimate of the maximum height H to radius R aspect ratio (H/R) for which the model applies is $H/R \approx 7$. For enclosures with $H/R \lesssim 7$ the rising plume (located in the centre of the floor) is able to spread without reaching the sides of the enclosure and is always able to entrain relatively freely. A second geometrical limitation is that the vertical extent of the openings be small compared with the total height of the space.

A sensible ventilation strategy is to design and locate the inlet and outlet openings so that their effective area ensures that both (i) the height of the stratification is above the occupied zone and (ii) the volume flow rate meets the requirements for respiration, removal of carbon-dioxide, odours and excess heat over the range of typical wind speeds and internal heat gains expected. If the system is designed to meet these requirements under the conditions of no wind then these requirements will be exceeded when the wind is harnessed to assist the buoyancy-driven flow. By harnessing the wind, the depth and temperature of the upper layer may be reduced thus providing 'passive' cooling of the building fabric. However, a change in the wind direction may result in the upper openings being located in regions of positive wind pressure and the low-level openings in regions of negative wind pressure and as a consequence the wind and buoyancy forces will oppose one another. This case presents a number of interesting implications for natural ventilation in buildings, including multiple steady states for identical forcing conditions, and is at present under investigation.

The authors would like to thank the Building Research Establishment for their financial support of this project through the Department of the Environment's Energy Related Environmental Issues (EnREI) in Buildings programme. We would like to thank D. Page-Croft, B. Dean and D. Lipman for constructing the experimental apparatus and for their technical support. We are also grateful to Caspar Williams for technical support.

Appendix A

Consider the enclosure depicted in figure 1 in the absence of a buoyancy source and suppose the interior is stably stratified with two homogeneous layers: a lower layer of depth h and density ρ, and an upper layer of depth $H-h$ and density $\rho_1 < \rho$. If p_0 is the total external fluid pressure at the centre of the windward opening then the total external pressure at the centre of the leeward opening may be written as $p_0 - \rho g(H - d_c) - \Delta$, where Δ denotes the wind pressure drop. Assuming the total area of the upper and lower openings is small compared with the cross-sectional area of the enclosure, the interface will slowly rise as buoyant fluid drains out of the space. The internal fluid pressures p_1 and p_2 at the level of the upper and lower openings, respectively, are then linked hydrostatically such that

$$p_2 = p_1 + \rho_1 g(H - h - d_c) + \rho g(h - d_f), \tag{A 1}$$

where d_f denotes the vertical distance from the floor to the centre of the lower opening. Using Bernoulli's theorem we obtain the fluid speeds through the respective

openings, namely

$$U_W^2 = \frac{2}{\rho}(p_0 - p_2) \quad \text{and} \quad U_L^2 = \frac{2}{\rho_1}(p_1 - [p_0 - \rho g(H - d_c - d_f) - \Delta]). \tag{A 2}$$

Flows through ventilation openings are unlikely to be dissipationless and there will be an effective reduction in the opening area due to the vena contracta which forms downstream of the openings. Accordingly (A 2) is replaced by

$$U_W^2 = \frac{2}{\rho}C_e(p_0 - p_2) \quad \text{and} \quad U_L^2 = \frac{2}{\rho_1}C_D^2(p_1 - [p_0 - \rho g(H - d_c - d_f) - \Delta]), \tag{A 3}$$

where the coefficients C_e and C_D account for these losses. For an incompressible fluid, conservation of volume yields

$$Q = a_W U_W = a_L U_L. \tag{A 4}$$

Eliminating p_0 and p_1 from (A 1) and (A 3) and using (A 4), for Boussinesq flows we obtain

$$Q = a_W a_L \left(\frac{2C_e C_D^2}{C_e a_W^2 + C_D^2 a_L^2}\right)^{1/2} (g'(H - h - d_c) + \Delta/\rho)^{1/2}, \tag{A 5}$$

cf. (3)–(5). Due to the relationship between pressure and velocity ($p \sim U^2$) we see from (A 5) that the buoyancy-produced velocity $\sqrt{g'(H - h - d_c)}$ and wind-produced velocity $\sqrt{\Delta/\rho}$ combine in a Pythagorean relationship.

Appendix B

Following Hunt & Kaye (2000), a plume with source conditions (Q_{p0}, M_0, B_0) and origin at $x = 0$ may be replaced with an equivalent, point-source pure plume with source conditions $(0, 0, B_0)$ at a virtual origin $x = -x_v$ located behind the actual source where

$$\frac{x_v}{\left[\dfrac{5}{6\alpha_G\sqrt{2}\pi^{1/2}}\dfrac{Q_0}{M_0^{1/2}}\right]} = \Gamma^{-1/5}(1 - \delta) \quad \text{for} \quad \Gamma > 1/2, \tag{B 1}$$

$$\delta = \frac{3}{5}\sum_{n=1}^{\infty}\left(\frac{\phi^n}{5^{n-1}n!(10n-3)}\prod_{m=1}^{n}[1 + 5(m-1)]\right), \tag{B 2}$$

$$\phi = \frac{\Gamma - 1}{\Gamma}, \tag{B 3}$$

and the dimensionless parameter Γ is determined from the source conditions of the plume

$$\Gamma = \frac{5}{2^{7/2}\alpha_G\pi^{1/2}}\left(\frac{Q_{p0}^2 B_0}{M_0^{5/2}}\right). \tag{B 4}$$

We make the assumption that the exit velocity profile of the (circular) nozzle is uniform so that $M_0 = 4Q_0^2/\pi D^2$, where D denotes the nozzle diameter, and hence

$$\frac{x_v}{D} = \frac{5}{6\alpha_G 2^{3/2}}\Gamma^{-1/5}(1 - \delta). \tag{B 5}$$

This assumption is reasonable on account of the turbulent flow observed at the outlet of the nozzle. Equations (B 1)–(B 5) are developed using an approach similar to Morton (1959) and represent a solution of the plume conservation equations

$$\frac{\mathrm{d}Q_p}{\mathrm{d}x} = 2^{3/2}\pi^{1/2}\alpha_G M^{1/2}, \quad \frac{\mathrm{d}M}{\mathrm{d}x} = \frac{Q_p B}{M} \quad \text{and} \quad \frac{\mathrm{d}B}{\mathrm{d}x} = 0 \tag{B 6}$$

(in this case for Gaussian profiles, which is a more accurate representation of the experimental plumes) subject to the intial conditions $Q = Q_{p0}, M = M_0$ and $B = B_0$ at $x = 0$. In Morton's (1959) analysis, the flow above the source (Q_{p0}, M_0, B_0) is related to an equivalent point-source-forced plume $(0, \gamma M_0, B_0)$ with modified momentum γM_0, where $\gamma = (1 - \Gamma)^{1/5}$. Source conditions for the saline plumes in the experiments typically lead to $\Gamma > 1$. In this case Morton's (1959) theoretical description is physically unrealistic, and differs from the analysis of Hunt & Kaye (2000), as the initial momentum of Morton's virtual source is directed downwards.

Corrections for the non-ideal source conditions were made by summing a sufficient number of terms in (B 2) to ensure that the position of the virtual origin was determined at least to the degree of accuracy with which the interface heights were measured.

REFERENCES

Baines, W. D. 1983 A technique for the direct measurement of volume flux for a plume. *J. Fluid Mech.* **132**, 247–256.

Baines, W. D. & Turner, J. S. 1968 Turbulent buoyant convection from a source in a confined region. *J. Fluid Mech.* **37**, 51–80.

Baker, N. & Linden, P. F. 1991 Physical models of air flows – a new design tool. In *Atrium Buildings Architecture and Engineering* (ed. F. Mills), pp. 13–22.

Batchelor, G. K. 1967 *An Introduction to Fluid Dynamics*. Cambridge University Press, Cambridge.

Cenedese, C. & Dalziel, S. B. 1998 Concentration and depth fields determined by the light transmitted through a dyed solution. In *Proc. 8th Intl Symp. on Flow Visualization* (ed. G. M. Carlomagno & I. Grant), Paper 061. ISBN 0953399109.

Cooper, P. & Linden, P. F. 1996 Natural ventilation of enclosures containing two buoyancy sources. *J. Fluid Mech.* **311**, 155–176.

Dalziel, S. B. 1993 Rayleigh-Taylor instability: experiments with image analysis. *Dyn. Atmos. Oceans* **20**, 127–153.

Flourentzou, F., Mass, J. van der & Roulet, C. A. 1996 Experiments in natural ventilation for passive cooling. In *Proc. 17th AIVC Conf., Gothenburg, Sweden*, pp. 121–134. Air Infiltration and Ventilation Centre, Coventry, UK.

Hunt, G. R. & Kaye, N. G. 2000 Virtual origin correction for lazy turbulent plumes. *J. Fluid Mech.* (submitted).

Hunt, G. R. & Linden, P. F. 1996 The natural ventilation of an enclosure by the combined effects of buoyancy and wind. In *Proc. ROOMVENT '96, the Fifth Intl Conf. on Air Distribution in Rooms* (ed. S. Murkami), vol. 3, pp. 239–246. University of Tokyo.

Hunt, G. R. & Linden, P. F. 1997 Laboratory modelling of natural ventilation flows driven by the combined forces of buoyancy and wind. In *Proc. CIBSE National Conference*, October 1997, vol. 1, pp. 101–107.

Hunt, G. R. & Linden, P. F. 1998 Time-dependent displacement ventilation caused by variations in internal heat gains: application to a lecture theatre. In *Proc. ROOMVENT '98, the 6th Intl Conf. on Air Distribution in Rooms, Stockholm, Sweden* (ed. E. Mundt & T. G. Malmstrom), vol. 2, pp. 203–210. KTH Stockholm.

Hunt, G. R. & Linden, P. F. 1999 The fluid mechanics of natural ventilation-displacement ventilation by buoyancy-driven flows assisted by wind. *Building Environ.* **36**, 707–720.

Hunt, G. R. & Linden, P. F. 2001 Steady-state stratified and mixing ventilation flows driven by the opposing forces of wind and buoyancy. *J. Fluid. Mech.* (submitted).

Kaye, N. G. 1998 Interaction of turbulent plumes. PhD thesis, University of Cambridge.

Linden, P. F. 1999 The fluid mechanics of natural ventilation. *Ann. Rev. Fluid Mech.* **31**, 201–238.

Linden, P. F. & Cooper, P. 1996 Multiple sources of buoyancy in a naturally ventilated enclosure. *J. Fluid Mech.* **311**, 177–192.

Linden, P. F., Lane-Serff, G. F. & Smeed, D. A. 1990 Emptying filling boxes: the fluid mechanics of natural ventilation. *J. Fluid Mech.* **212**, 300–335.

Morton, B. R. 1959 Forced plumes. *J. Fluid Mech.* **5**, 151–163.

Morton, B. R., Taylor, G. I. & Turner, J. S. 1956 Turbulent gravitational convection from maintained and instantaneous sources. *Proc. R. Soc. Lond.* A **234**, 1–23.

Orme, M., Liddament, M. & Wilson, A. 1994 An analysis and data summary of the AIVC's numerical database. *Tech. Note* 44, pp. 73–89. The Air Infiltration and Ventilation Centre, Coventry, UK.

Turner, J. S. 1986 Turbulent entrainment: the development of the entrainment assumption, and its application to geophysical flows. *J. Fluid Mech.* **173**, 431–471.

Ward-Smith, A. J. 1980 *Internal Fluid Flow – the Fluid Dynamics of Flow in Pipes and Ducts*. Clarenden.